nature immunology

ARTICLES

https://doi.org/10.1038/s41590-022-01274-3

Check for updates

PD-1 directed immunotherapy alters Tfh and humoral immune responses to seasonal influenza vaccine

Ramin Sedaghat Herati[1,11]✉, David A. Knorr[2,3,11], Laura A. Vella[4,5], Luisa Victoria Silva[5], Lakshmi Chilukuri[3], Sokratis A. Apostolidis[5,6], Alexander C. Huang[5,6,7], Alexander Muselman[6,10], Sasikanth Manne[5,8], Oliva Kuthuru[5,8], Ryan P. Staupe[5], Sharon A. Adamski[5,8], Senthil Kannan[9], Raj K. Kurupati[9], Hildegund C. J. Ertl[9], Jeffrey L. Wong[2,3], Stylianos Bournazos[2], Suzanne McGettigan[6,7], Lynn M. Schuchter[6,7], Ritesh R. Kotecha[3], Samuel A. Funt[3], Martin H. Voss[3], Robert J. Motzer[3], Chung-Han Lee[3], Dean F. Bajorin[3], Tara C. Mitchell[6,7], Jeffrey V. Ravetch[2]✉ and E. John Wherry[5,8]✉

Anti-programmed death-1 (anti-PD-1) immunotherapy reinvigorates CD8 T cell responses in patients with cancer but PD-1 is also expressed by other immune cells, including follicular helper CD4 T cells (Tfh) which are involved in germinal centre responses. Little is known, however, about the effects of anti-PD-1 immunotherapy on noncancer immune responses in humans. To investigate this question, we examined the impact of anti-PD-1 immunotherapy on the Tfh–B cell axis responding to unrelated viral antigens. Following influenza vaccination, a subset of adults receiving anti-PD-1 had more robust circulating Tfh responses than adults not receiving immunotherapy. PD-1 pathway blockade resulted in transcriptional signatures of increased cellular proliferation in circulating Tfh and responding B cells compared with controls. These latter observations suggest an underlying change in the Tfh–B cell and germinal centre axis in a subset of immunotherapy patients. Together, these results demonstrate dynamic effects of anti-PD-1 therapy on influenza vaccine responses and highlight analytical vaccination as an approach that may reveal underlying immune predisposition to adverse events.

Cancer immunotherapy has revolutionized our ability to target and redirect immune system activity to treat malignancies. PD-1 (CD279) expressed on T cells during activation and exhaustion is the most common target of cancer immunotherapy[1]. Blockade of PD-1 signaling using anti-PD-1 or anti-Programmed Death-Ligand1 (anti-PD-L1) immunotherapy has been associated with improved survival or cure in several different types of malignancies, in part due to the reinvigoration of exhausted CD8 T cells[2]. However, PD-1 is expressed by other immune cells including Tfh that provide help to B cells in the germinal centre (GC), thereby enabling affinity-matured, long-lived antibody responses[3,4]. Indeed, Tfh cells in secondary lymphoid tissue have high PD-1 expression in humans[3,5–7]. Little is known, however, about the effects of anti-PD-1 immunotherapy on Tfh or on related events including the outcomes of Tfh–B cell interactions and GC-dependent immune responses. Moreover, approximately 50% of patients on anti-PD-1 immunotherapy develop immune-related adverse events (irAEs)[8–11]. At least some of these irAEs have been postulated to be linked to autoreactive humoral responses[12–14], but precise mechanisms remain poorly defined. Thus, there is a need to better understand the immunological effects of anti-PD-1 on parts of the immune system not directly related to the on-tumor effects.

The main goal of immunotherapy for cancer or other diseases is to treat the tumour or affected tissue or system. As a result, the impact of immunotherapies on immune responses unrelated to disease have received less attention. For example, the Tfh–B cell axis is central for vaccine responses, yet the effects of anti-PD-1 therapy on vaccine-induced Tfh and humoral responses have not been extensively studied in humans. Indeed, examining immune responses to vaccine antigens in the setting of PD-1 blockade may provide insights into the function of PD-1 in the 'normal' immune system and potentially reveal new opportunities to improve vaccination or understand the role of the PD-1 pathway in other diseases. A small number of studies have evaluated influenza vaccines, mainly for safety or serology in the setting of anti-PD-1 immunotherapy[15–20]. However, no information exists on how perturbing the PD-1 pathway in humans impacts Tfh responses to vaccination or the Tfh–B cell axis responsible for generating high-quality antibodies.

To examine these questions, we used influenza vaccination in human patients with cancer to directly investigate the effects of

[1]Department of Medicine, New York University School of Medicine, New York, NY, USA. [2]Laboratory of Molecular Genetics and Immunology, Rockefeller University, New York, NY, USA. [3]Department of Medicine, Memorial Sloan Kettering Cancer Center, New York, NY, USA. [4]Department of Pediatrics, Children's Hospital of Philadelphia, Philadelphia, PA, USA. [5]Institute for Immunology University of Pennsylvania School of Medicine, Philadelphia, PA, USA. [6]Department of Medicine, University of Pennsylvania School of Medicine, Philadelphia, PA, USA. [7]Abramson Cancer Center, Division of Hematology/Oncology, University of Pennsylvania School of Medicine, Philadelphia, PA, USA. [8]Department of Systems Pharmacology and Translational Therapeutics, University of Pennsylvania School of Medicine, Philadelphia, PA, USA. [9]Wistar Institute, Philadelphia, PA, USA. [10]Present address: Department of Immunology, Stanford University, Stanford, CA, USA. [11]These authors contributed equally Ramin Sedaghat Herati, David A. Knorr. ✉e-mail: ramin.herati@nyulangone.org; ravetch@mail.rockefeller.edu; wherry@pennmedicine.upenn.edu

anti-PD-1 immunotherapy on Tfh and B cell responses to noncancer antigens. Specifically, we examined responses of the circulating subset of PD-1$^+$ CXCR5$^+$ CD4 cells, termed circulating Tfh (cTfh), which share phenotypic and functional characteristics of lymphoid Tfh[5,21–25]. These studies demonstrate that anti-PD-1 treatment was associated with more robust vaccine-induced cTfh responses and increased proliferation of responding cTfh and B cells including antibody secreting cells (ASCs). Mechanistically, this increased cTfh and ASC proliferation was coupled to reduced transcriptional signatures of cytokine signaling including IL-2/STAT5 in cTfh and TNF/NFkB in ASCs. These anti-PD-1-induced changes in vaccine-responding cTfh and B cells were associated with greater increase in titer but lower affinity and lower sialylation of neutralizing influenza-specific antibodies compared with those not receiving immunotherapy. Increases in serum CXCL13 following vaccination in the presence of anti-PD-1 implicated altered GC activity. Finally, although vaccination does not provoke immunotherapy-associated complications[17], a subset of participants with robust changes in cTfh were enriched for previous (or future) irAEs associated with immunotherapy, suggesting an underlying change in Tfh–B cell, humoral and/or GC activity. This latter observation points to a potential common signature or baseline immune state altered by PD-1 that impacts vaccination and autoreactivity. Moreover, these studies highlight the potential to use analytical vaccination to detect these changes, possibly identifying patients with higher likelihood for irAEs. Together, these data demonstrate that anti-PD-1 immunotherapy has broad effects on the Tfh–B cell axis with major implications for vaccination, humoral responses and changes in baseline immune health.

Results

Anti-PD-1 is associated with increased cellular responses to vaccination. Anti-PD-1 immunotherapy with nivolumab or pembrolizumab is given over months or even years[1] with the intention of enhancing the immune response to cancer. The effects of long-term disruption of the PD-1 pathway on immune responses to other antigens including humoral responses to vaccines that involve PD-1-expressing Tfh remain poorly understood. To address this question, we enrolled adults with renal cell carcinoma or urothelial carcinoma who were receiving immunotherapy (Cohort 1; Supplementary Table 1) and were due to receive seasonal inactivated influenza vaccine. Participants were divided into two groups: non-anti-PD-1-based therapy ($n=10$, median age=65) or anti-PD-1-based therapy ($n=29$, median age=71.5). Given the importance of Programmed Death-Ligand 2 signaling in the humoral response[26,27], we considered participants who received anti-Programmed Death-Ligand 1 as members of the non-anti-PD-1 group. In a second, independently generated cohort at a different institution, we enrolled adults with melanoma receiving immunotherapy ($n=30$, median age=61.5) and healthy adults not receiving immunotherapy ($n=27$, median age=33) (Cohort 2; Supplementary Table 2). Participants received influenza vaccination on the same day as immunotherapy infusion (median of cycle 12 of anti-PD-1 for Cohort 1 and cycle 7 for Cohort 2; Extended Data Fig. 1a,b). Blood was drawn on the day of vaccination (baseline), 1 week later and again 3–6 weeks after vaccination (late) (Extended Data Fig. 1a), as has been done previously[21,22,25,28].

In healthy adults, CXCR5$^+$ PD-1$^+$ cTfh expressing the activation markers Inducible Costimulator (ICOS, CD278) and CD38 expand 1 week after influenza vaccination and this population contains influenza-specific CD4 T cells[25]. We therefore first asked whether anti-PD-1 immunotherapy alters the cTfh response to the vaccine. To avoid bias of using PD-1 itself in detection of cTfh due to treatment with therapeutic anti-PD-1 antibodies, we used a broader definition of non-naive CXCR5$^+$ CD4 T cells that coexpressed ICOS and CD38 (ICOS$^+$CD38$^+$ cTfh) to identify responding cTfh in this study (Extended Data Fig. 1c–e). Following vaccination in Cohort 1, there was a 2.6-fold-induction of ICOS$^+$CD38$^+$ cTfh in patients with cancer receiving anti-PD-1 compared with a 1.1-fold-change in patients with cancer on therapies other than anti-PD-1 ($P=0.013$, Wilcoxon test; Fig. 1b), demonstrating that anti-PD-1 therapy is associated with augmented cTfh responses to influenza vaccination.

We examined an independent cohort of patients with melanoma receiving anti-PD-1 immunotherapy (Cohort 2; Supplementary Table 1). Again, anti-PD-1 therapy was associated with more robust increases in cTfh responses compared with healthy control participants 1 week after vaccination ($P=0.05$, Wilcoxon test), with responses returning to baseline by the late time point (Fig. 1c,d and Extended Data Fig. 1f–h). We also confirmed that using PD-1 in the definition of cTfh resulted in similar observations (Extended Data Fig. 1i–k). The increase in the cTfh response was not associated with more recent initiation of anti-PD-1 therapy (Extended Data Fig. 1l) and was unlikely to be due to age-related differences between participants (Extended Data Fig. 1m,n). Further subsetting based on CCR6 and CXCR3, as described previously[23], did not identify differences between treatment groups (Extended Data Fig. 1o). Finally, we considered other regulators of the B cell response. In particular, T follicular regulatory cells (Tfr) phenotypically resemble Tfh but express Foxp3 and can regulate Tfh–B cell interactions[29]. There was a greater decrease in the frequency of circulating Tfr (cTfr) in the anti-PD-1-treated participants than in the healthy adults in Cohort 2 (Extended Data Fig. 1p–r). However, this change could reflect dilution of cTfr by the ICOS$^+$CD38$^+$ CXCR5$^+$ cTfh or perhaps be due to altered kinetics. Given the structure of the study, it was not possible to assess cTfh and cTfr responses at different time points. Nonetheless, these data indicate that anti-PD-1 treatment was associated with an augmented numerical response of cTfh in a subset of patients 1 week after influenza vaccination.

We next asked if the B cell response to vaccination was affected by anti-PD-1 therapy. Although the plasmablast frequency was not higher in the anti-PD-1 group following vaccination, there was a subset of anti-PD-1 participants with robust induction of plasmablasts 1 week after vaccination, (Fig. 1e and Extended Data Fig. 2a–d). Correlations have been observed previously between plasmablast and cTfh responses to influenza vaccination[22,25]. Here, the plasmablast response correlated with ICOS$^+$CD38$^+$ cTfh responses 1 week after vaccination in the anti-PD-1 group in both cohorts (Fig. 1f). These data suggest that anti-PD-1 therapy alters Tfh–B cell interactions, likely in secondary lymphoid tissues, resulting in higher frequencies of both cTfh and plasmablasts in the peripheral blood following vaccination.

One biomarker of GC activity in lymphoid tissue is plasma CXCL13 (ref. [30]). We observed weak induction of plasma CXCL13 in healthy adults 1 week after influenza vaccination (Fig. 1g), consistent with previous studies showing that influenza vaccination induced only modest changes in this chemokine detectable in blood thought to be related to the relatively weak immune response to this vaccine[30]. In contrast, however, anti-PD-1-treated participants had substantial induction of plasma CXCL13 1 week after vaccine compared with baseline in both cohorts (Fig. 1g,h and Extended Data Fig. 2e–g). Although this CXCL13 in the blood did not correlate strongly with the cTfh or plasmablast response, there was a correlation with later antibody responses (Extended Data Fig. 2h). Collectively, these data reveal a robust enhancement of vaccine-induced cTfh, plasmablast and likely GC activity in the presence of anti-PD-1 therapy.

Anti-PD-1 altered antibody responses. Humoral responses to influenza vaccination are typically assessed by hemagglutinin inhibitory (HAI) antibody titers, which are a correlate of protection following vaccination[31]. Thus, we investigated whether anti-PD-1 therapy impacted the induction of HAI titers. We focused on Cohort 2 because of the larger number of individuals available for analysis.

We first examined the fold-change in the HAI antibody titer at the 3–6-week time point compared with the baseline titer.

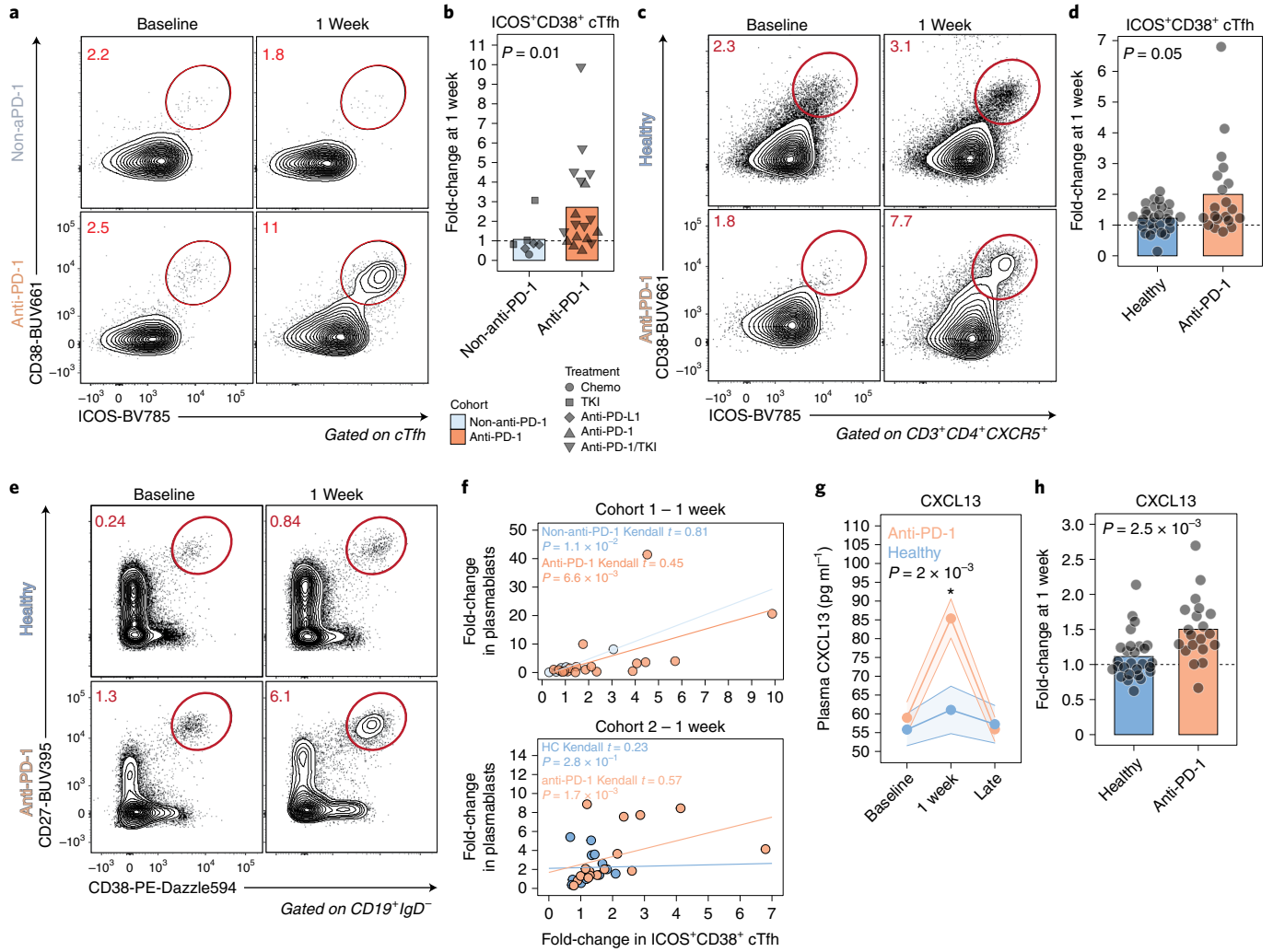

Fig. 1 | Anti-PD-1 treatment is associated with enhanced cTfh, B cell and GC responses following influenza vaccination. a, cTfh were profiled for expression of ICOS and CD38 at baseline and at 1 week after influenza vaccine in Cohort 1. **b**, ICOS$^+$CD38$^+$ cTfh fold-change at 1 week in Cohort 1 (P=0.01, two-sided Wilcoxon test; anti-PD-1 (n=18) versus non-anti-PD-1 (n=7)). **c**, Patients with melanoma were recruited in Cohort 2 and profiled following influenza vaccination. cTfh responses shown at baseline and 1 week. **d**, ICOS$^+$CD38$^+$ cTfh fold-change at 1 week compared with baseline in Cohort 2 (P=0.05, two-sided Wilcoxon test; anti-PD-1 (n=20) versus healthy (n=27)). **e**, Plasmablast responses after influenza vaccination in Cohort 2. **f**, Kendall correlation between plasmablasts and ICOS$^+$CD38$^+$ cTfh at 1 week for Cohorts 1 and 2. **g**, Plasma CXCL13 over time (P=2×10^{-3} for anti-PD-1 at 1 week compared with baseline, two-way ANOVA with Tukey's post-test). Data are presented as mean value (point) ±s.e.m. (shaded area). **h**, Plasma CXCL13 fold-change at 1 week in Cohort 2 (P=2.5×10^{-3}, two-sided t-test; anti-PD-1 (n=20) versus healthy (n=27)). HC, healthy controls; TKI, tyrosine kinase inhibitor.

Indeed, across all three strains of influenza included in the vaccine, neutralizing antibody titers increased by a median of 4-fold in the presence of anti-PD-1 compared with 2-fold in the absence of anti-PD-1 (Fig. 2a and Extended Data Fig. 3a). Most anti-PD-1-treated adults had antibody titers of >1:40 following vaccination and were thus seroprotected, similar to healthy adults, indicating no clinical deficiency in the outcome of vaccination in this setting (Fig. 2b). The absolute HAI titer was similar between the anti-PD-1 and non-anti-PD-1 at the late time point, and the difference in fold-induction reflected slightly lower baseline HAI titers in the anti-PD-1 group than in the non-anti-PD-1 group (Fig. 2c and Extended Data Fig. 3b). These data are consistent with a previous study showing increases in influenza-specific antibodies in patients vaccinated while on anti-PD-1 therapy[15]. In Cohort 1, there were similar trends, but these differences in HAI titers in Cohort 1 did not reach statistical significance, perhaps because of a smaller number of participants, more varied treatment regimens or the effects of previous cancer therapy (Extended Data Fig. 3c,d). In this setting, correlations between cTfh or B cell responses and HAI titers were not apparent (Extended Data Fig. 3e). The differences in antibody observed in Cohort 2 were unlikely to be due to the differences in age between the two groups, since independent analyses did not reveal age-associated differences in influenza-specific neutralizing antibodies at baseline (Extended Data Fig. 3f). Together, these data show that the increases in cTfh, plasmablast and CXCL13 responses were associated with quantitatively increased antibody responses in the setting of anti-PD-1 compared with participants not receiving anti-PD-1 therapy.

Antibodies provide protection by being present at sufficient quantities and by undergoing qualitative improvements during the T cell-dependent phase of induction in lymphoid tissues. However, because the data above revealed a quantitative impact of anti-PD-1 on induction of antibody following vaccination, but endpoint HAI titers were similar, we next wanted to investigate potential qualitative effects of anti-PD-1 treatment on antibody responses. For example, antibody effector function is dictated

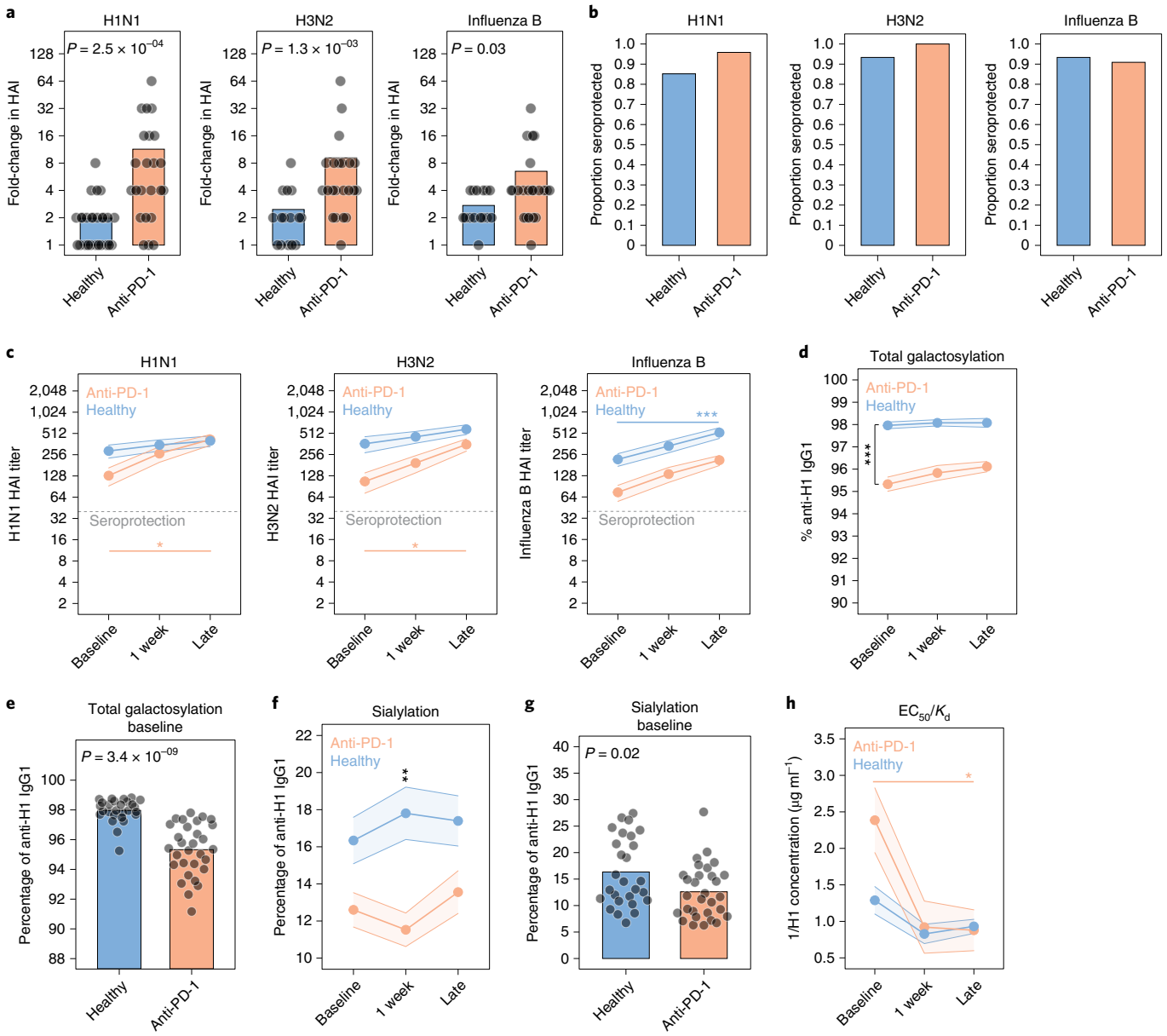

Fig. 2 | Anti-HA antibodies were quantitatively similar but qualitatively worse with anti-PD-1. a, HAI as fold-change at the late time point compared with baseline for each strain. Nominal *P* values from two-sided *t*-test comparisons are shown (anti-PD-1 ($n=24$) versus healthy ($n=27$ for H1N1, $n=15$ for H3N2 and FluB)). **b**, Seroprotection for each strain, shown as the proportion of participants who achieved an HAI titer of 1:40 or higher 21–42 d after vaccination. **c**, H1 inhibition titers determined for the H1N1 (*$P=0.01$; anti-PD-1 baseline versus anti-PD-1 late; two-way ANOVA with Tukey's), H3N2 (*$P=0.03$; anti-PD-1 baseline versus anti-PD-1 late; two-way ANOVA with Tukey's) and influenza B strains (***$P=7.1\times10^{-4}$; healthy baseline versus healthy late; two-way ANOVA with Tukey's). Data are presented as mean value (point) ± s.e.m. (shaded area). **d**, Proportion of anti-H1 IgG1 antibodies galactosylated (***$P=1.8\times10^{-12}$, two-way ANOVA with Tukey's; anti-PD-1 versus healthy at baseline). Data are presented as mean value (point) ± s.e.m. (shaded area). **e**, Proportion of anti-H1 antibodies galactosylated at baseline ($P=3.4\times10^{-9}$, two-sided *t*-test; anti-PD-1 ($n=30$) versus healthy ($n=27$)). **f**, Sialylation for anti-H1 IgG1 antibodies (**$P=7.1\times10^{-3}$, two-way ANOVA with Tukey's; comparison of anti-PD-1 versus healthy at 1 week). Data are presented as mean value (point) ± s.e.m. (shaded area). **g**, Proportion of anti-H1 antibodies sialylated at baseline ($P=0.02$, two-sided *t*-test; anti-PD-1 ($n=30$) versus healthy ($n=27$)). **h**, Affinity determined as EC_{50}/K_d (*$P=0.02$, two-way ANOVA with Tukey's; anti-PD-1 at baseline versus late). Data are presented as mean value (point) ± s.e.m. (shaded area).

by two important components of the antibody Fc fragment, both the amino acid sequence (for example, IgG subclass IgG1–4) and the composition of the conserved N-linked glycan at asparagine position 297 (ref. [32]). We previously demonstrated that changes to anti-hemagglutinin (HA) glycoforms, in particular increased total sialylation of influenza-specific IgG, drove B cell affinity selection and determined the efficacy of influenza vaccination[33]. We therefore investigated how disruption of the PD-1 pathway impacted antibody glycosylation and subsequent affinity. We focused on the antibody response to hemagglutinin (H1), the primary target of the antibody response in vaccinated individuals[34]. IgG subclass and glycan distribution of antigen-specific IgG were evaluated using mass spectrometry[33]. Overall, anti-H1 antibodies were enriched for the IgG1 subclass, with less IgG2 and IgG3/4 in the setting of anti-PD-1 compared with controls (Extended Data Fig. 4a; $P=9\times10^{-3}$, two-way analysis of variance (ANOVA) with Sidak's post-test).

We next investigated how anti-PD-1 treatment impacted antibody glycosylation. Afucosylation of antibodies results in enhanced antibody-dependent cytotoxicity[32], but was not affected by anti-PD-1 treatment (Extended Data Fig. 4b). Sialylation and galactosylation are two additional Fc glycosylation events that can regulate antibody function. Sialylated antibodies conferred improved protection to influenza in vivo[33] and galactosylation is a prerequisite for sialylation[32]. Indeed, sialylation and galactosylation of anti-H1 antibodies were correlated for both anti-PD-1-treated and nontreated groups (Extended Data Fig. 4c). However, the anti-PD-1-treated patients had lower total galactosylation (Fig. 2d,e) and sialylation (Fig. 2f,g) of anti-H1 antibodies than non-anti-PD-1-treated participants at baseline and after vaccination, and these observations were consistent across all immunoglobulin subclasses (Extended Data Fig. 4d–f). In Cohort 1, anti-PD-1-treated participants had lower galactosylation and sialylation of anti-H1 antibodies at baseline (Extended Data Fig. 4g–j). In previous studies, we found similar changes in glycosylation between antigen-specific and total antibodies[33,35,36]. We therefore focused here on anti-H1 antibodies because these are a major mechanism of vaccine-induced protection. However, we observed similar changes in glycosylation patterns on anti-H1 antibodies of all antibody subclasses examined, suggesting a broad impact on antibody glycosylation (Extended Data Fig. 4d,f). Altogether, these data identify an effect of anti-PD-1 therapy on sialylation of anti-H1 antibodies at baseline and after vaccination, effects that might be predicted to impact the quality of influenza-specific antibodies.

To test whether altered antibody glycosylation in the setting of anti-PD-1 treatment had functional consequences, we next examined antibody affinity. Sialylation of antigen-specific IgG and immune complexes contributes to affinity maturation through FcγRIIb-mediated modulation of GC B cell selection favoring higher affinity clones[33]. Thus, lower sialylation in the context of anti-PD-1 was predicted to impact subsequent antibody affinity. Indeed, baseline antibody affinity was lower in patients on anti-PD-1 compared with healthy controls (Fig. 2h and Extended Data Fig. 4k). Using a second assay that estimates affinity based on binding to low- versus high-density antigen[33], we confirmed that anti-PD-1-treated participants had lower affinity IgG1 at baseline (Extended Data Fig. 4l–n). Collectively, these data identify both quantitative and qualitative changes in antibody responses to influenza vaccine associated with blockade of PD-1. Because some of these changes were present before yearly vaccination, these data suggest perhaps an underlying impact of anti-PD-1 therapy on influenza-specific immune memory, in addition to the effects on the responses provoked by the vaccination studied here.

Given these changes in antibody, we next investigated whether anti-PD-1 treatment was associated with changes in B cell subsets that responded to vaccination, including ASCs (gated as $CD19^+IgD^-CD71^+CD20^{lo}$) and activated B cells (ABCs; gated as $CD19^+IgD^-CD71^+CD20^{hi}$)[37]. Even before vaccination, anti-PD-1 therapy was associated with a higher frequency of circulating ASCs and reciprocally reduced ABC frequencies (Extended Data Fig. 4o,p). However, whereas ABCs only weakly correlated with $ICOS^+CD38^+$ cTfh, at baseline and after vaccination, ASC frequencies were positively correlated with $ICOS^+CD38^+$ Tfh in anti-PD-1 patients before and after vaccination (Extended Data Fig. 4q,r). Taken together, these data indicate that anti-PD-1 treatment is associated with alterations in B cell subsets at baseline and in vaccine-induced antibody quantity and quality. Moreover, these alterations before vaccination suggest that treatment with anti-PD-1 may alter the baseline Tfh–B cell and humoral immune set point in these individuals.

Anti-PD-1 is associated with dynamic transcriptional effects. To further interrogate the effects of anti-PD-1 on immune responses to influenza vaccination, we performed transcriptional profiling on sorted $ICOS^+CD38^+$ cTfh, ABCs, ASCs or naïve B cells (gated as $CD19^+IgD^+CD27^{lo}$) from participants in Cohort 2. Sample distribution in *t*-distributed stochastic neighbor embedding (*t*-SNE) space was driven primarily by cell subset and minimally by treatment or timing relative to vaccination (Extended Data Fig. 5a–e). However, at 1 week post vaccination, transcriptional differences were readily apparent in $ICOS^+CD38^+$ cTfh from anti-PD-1-treated adults compared with $ICOS^+CD38^+$ cTfh from healthy adults including upregulation of genes such as *MKI67* and *ESPL1*, indicating recent proliferation[38], and lower expression of genes including *IFI44L*, *OASL* and *TNFRSF1B* (Fig. 3a and Supplementary Table 5), suggesting reduced response to interferon signaling[39,40]. A similar upregulation of *ESPL1*, *MKI67* and other cell cycle genes was observed in anti-PD-1-induced 'burned-out' CD8 T cells in patients with cancer[41]. Gene ontology (GO) term enrichment highlighted proliferation and cell cycle in the transcriptional signatures of $ICOS^+CD38^+$ cTfh from anti-PD-1-treated participants following vaccination compared with leukocyte activation, migration, as well as cytokine production and signaling in the control group (Fig. 3b and Extended Data Fig. 5f). Indeed, Ki67 protein expression 1 week after vaccination correlated with the fold-change in the $ICOS^+CD38^+$ cTfh (Extended Data Fig. 5g), supporting the notion that anti-PD-1 therapy was associated with an enhanced proliferative cTfh response after immunization.

Similarly, ASCs from vaccinated anti-PD-1-treated participants upregulated genes such as *AURKB*, *BUB1* and *ESPL1*, consistent with greater proliferation relative to ASCs from healthy adults (Fig. 3c and Extended Data Fig. 5h), and had terms for 'cell cycle' and 'mitotic cell division' by GO (Fig. 3d and Extended Data Fig. 5i). ASCs from the anti-PD-1 group also had higher expression of *CCL2* and *IL18RAP*, but lower expression of *IFNGR2*, *DUSP1* and *KCNA3*. Moreover, upregulation of *ARID1A* in $ICOS^+CD38^+$ cTfh and *SMARCD1* in ASCs from the anti-PD-1 group also suggested a potential impact on SWI/SNF complex use in these cells responding to vaccination in the absence of normal PD-1 signaling. These proliferation-related genes were not observed before vaccination (Extended Data Fig. 5i,j).

We next performed gene set enrichment analysis (GSEA)[42] for both cTfh and ASCs to identify pathways altered due to anti-PD-1 at 1 week after vaccination. For the $ICOS^+CD38^+$ cTfh, we identified four gene sets that were enriched in the anti-PD-1 participants, all of which were associated with proliferation, whereas 27 gene sets were enriched in the controls (Fig. 3e). Indeed, enrichments of gene sets associated with proliferation were also identified in the ASC and ABC subsets of anti-PD-1 participants 1 week after vaccination (Fig. 3f–h and Extended Data Fig. 6a,b). These data indicate that anti-PD-1 drove greater activation and proliferation of cTfh and B cell populations during the vaccine response.

In addition to the genes and pathways upregulated in the presence of anti-PD-1, genes and pathways downregulated or that failed to be induced following influenza vaccination in anti-PD-1 patients were also of interest. Indeed, anti-PD-1 was associated with relative reduction in several pathways of direct relevance for cTfh biology in vaccine-responding $ICOS^+CD38^+$ cTfh. First, the STAT5/Blimp-1 axis is a negative regulator of Tfh differentiation and function, in part through antagonism of the Tfh-driving transcription factor Bcl6 (refs. [43,44]). Here, anti-PD-1 treatment was associated with downregulation of IL-2/STAT5 signaling in activated cTfh (Fig. 3i) consistent with the enhanced cTfh response in a subset of anti-PD-1 patients. Moreover, enrichment for the IL-2/STAT5 gene set was negatively correlated with $ICOS^+CD38^+$ cTfh frequency in anti-PD-1 patients but not healthy controls, consistent with a regulatory effect of this pathway on Tfh activation and/or expansion that is revealed by anti-PD-1 treatment (Extended Data Fig. 6c). Other Tfh-regulating pathways, such as TGF-β signaling and apoptosis, were also downregulated in the setting of anti-PD-1 treatment (Fig. 3e).

Downregulation of regulatory signaling pathways such as IL-2/STAT5 signaling that normally impede Tfh activity in the setting of anti-PD-1 may help explain the greater influenza vaccine-induced cTfh and antibody responses in the setting of anti-PD-1 (Fig. 2).

A second relevant transcriptional imprint of anti-PD-1 treatment was downregulation of genes involved in the TNF/NFkB pathway. These changes were of interest at least in part because TNF and NFkB signaling are regulators of cTfh biology[45]. In the setting of anti-PD-1 treatment, signatures of TNF/NFkB-related genes in ICOS$^+$CD38$^+$ cTfh were highly biased to the control participants (Fig. 3e), suggesting that anti-PD-1 treatment impaired efficient use of TNF/NFkB signaling in vaccine-responding activated cTfh. A similar picture emerged for ASCs (Fig. 3f), suggesting a coordinated set of biological pathways impacted by anti-PD-1 therapy for both cTfh and ASCs. Thus, these data indicate that anti-PD-1 may alter the humoral, cTfh and likely GC responses by dysregulating control of proliferation and altered sensing of key cytokine circuits needed for proper Tfh control of humoral immunity.

cTfh responses are predictive of irAEs. A major limitation of current checkpoint blockade in cancer immunotherapy is the development of irAEs[12,13]. Although the underlying mechanisms have been unclear, one possibility is dysregulated GC-dependent immune responses including CD4 T cells (for example, Tfh) and antibody responses[46,47]. Thus, we hypothesized that differences in Tfh biology during anti-PD-1 therapy may offer insights into the mechanisms of irAE.

To test this idea, we focused on participants in Cohort 2 where anti-PD-1 was predominantly used as monotherapy, and considered irAEs irrespective of timing to influenza vaccination (Extended Data Fig. 7a and Supplementary Table 6). We considered whether messenger RNA profiling of ICOS$^+$CD38$^+$ cTfh at baseline could identify characteristics of those who had an irAE versus those who did not have any irAEs. Patients with irAEs had slightly more transcripts for genes associated with cellular activation, such as *PDCD1* and *ICOS*, relative to patients who did not have irAEs, although these differences were not statistically significant (Extended Data Fig. 7b,c). However, we observed higher expression of ICOS protein and PD-1 protein, using αIgG4 as a proxy for PD-1 (ref. [2]), in anti-PD-1-treated adults with irAEs compared with anti-PD-1-treated adults who did not have irAEs (Extended Data Fig. 7d–f). Transcriptional analysis of ICOS$^+$CD38$^+$ cTfh revealed 18 genes upregulated in activated cTfh from patients with irAEs, including *KIF2C*, *MKI67* and *BIRC5*, compared with patients without irAEs (Fig. 4a, Extended Data Fig. 7g and Supplementary Table 7). Consistent with these proliferation-associated genes, GO analysis also revealed enrichment for terms related to cell cycle and cellular activation in patients with irAEs (Extended Data Fig. 7h). Other genes of potential interest were also revealed, including the cytokine *IL32*, the splicing factor *XAB2* and *CD52*, the target of alemtuzumab used to treat chronic lymphocytic leukaemia and multiple sclerosis[48], which were all more highly expressed in activated cTfh from anti-PD-1-treated adults with irAEs. In contrast, higher *ITGA5*, *CD82* and *FOS* were found in cTfh from anti-PD-1-treated adults without irAEs. These data indicated that, before influenza vaccination, ICOS$^+$CD38$^+$ cTfh in anti-PD-1-treated adults with irAEs were more activated than in anti-PD-1-treated adults without irAEs and anti-PD-1 therapy may engage additional biologically relevant pathways.

GSEA identified enrichment of G2M checkpoint and E2F targets in ICOS$^+$CD38$^+$ cTfh at baseline from participants with irAEs compared with those without irAEs (Fig. 4b), further supporting the idea that ICOS$^+$CD38$^+$ cTfh from patients with irAEs were more activated, even before influenza vaccination, compared with patients without irAEs. This observation is consistent with other reports that identified T cell activation as a predictor of irAEs[49]. In addition to proliferation-associated pathways, multiple other irAE-associated biologic pathway changes in cTfh were revealed, including downregulation of IL-2/STAT5, TNF/NFkB, IL6/JAK/STAT, IFN-γ and TGF-β signaling, consistent with the results above. Taken together, these data support the notion of an anti-PD-1-mediated rewiring of cTfh biology in patients with irAEs that includes increased activation and proliferation concomitant with blunting of cytokine pathway signaling.

These observations provoked the hypothesis that the post-influenza vaccine cTfh response might distinguish anti-PD-1 patients with irAEs from those without irAEs because of an underlying change in the global set point of Tfh regulation. To test this idea, we examined the magnitude of the ICOS$^+$CD38$^+$ cTfh increase 1 week following influenza vaccination in patients who did, or did not, have irAEs. Indeed, in patients with irAEs, influenza vaccination had a more robust ICOS$^+$CD38$^+$ cTfh response compared with patients without irAEs (~2.4-fold compared with 1.3-fold; Fig. 4c). A similar trend was seen in patients in Cohort 1 who were receiving anti-PD-1 monotherapy (Extended Data Fig. 7i). No difference was observed in the frequency of ICOS$^+$CD38$^+$ cTfh before vaccination (Extended Data Fig. 7j), suggesting a key role for the vaccine-induced perturbation in revealing this biology. Moreover, we did not observe increases in titers of anti-nuclear or anti-double-stranded DNA (anti-dsDNA) autoantibodies with anti-PD-1 therapy or in the setting of irAEs (Extended Data Fig. 7k,l). Thus, these observations suggest that anti-PD-1 therapy alters Tfh–B cell and likely underlying GC biology, at least in a subset of patients, and that these changes can alter the magnitude and quality of the response to vaccination. The alteration in this Tfh–B cell and GC axis correlates with propensity for anti-PD-1-associated irAEs and perhaps points to underlying rewiring of Tfh and GC biology contributing to these outcomes which may be more sensitive than general autoantibody measurements such as anti-nuclear or anti-dsDNA antibodies. Thus, using influenza vaccination as an 'analytical probe' of underlying changes in immune function revealed a proliferatively enhanced, but biologically altered, response to vaccination which also identified participants predisposed to irAEs.

Discussion

Checkpoint blockade therapies including anti-PD-1 antibodies are now a major tool in the arsenal for the treatment of cancer. Substantial effort has focused on the in vivo effects of anti-PD-1 therapy on the CD8 T cell response[1]. However, as evidenced by

Fig. 3 | Anti-PD-1 is associated with cellular proliferation and reduced IL-2/STAT5 signaling. a, Top and bottom 50 genes from differential expression analysis of ICOS$^+$CD38$^+$ cTfh at 1 week after vaccination. **b**, GO analysis shown for genes enriched in anti-PD-1 (peach) and those enriched in healthy (blue) for ICOS$^+$CD38$^+$ cTfh. *P* values from hypergeometric test with Benjamini–Hochberg *P* value correction. **c**, Top and bottom 50 genes from differential expression analysis of ASCs at 1 week after vaccination. **d**, GO analysis shown for genes enriched in anti-PD-1 (peach) and those enriched in healthy (blue) for ASCs. *P* values from hypergeometric test with Benjamini–Hochberg *P* value correction. **e**, GSEA for MSigDB Hallmark gene sets used to compare ICOS$^+$CD38$^+$ cTfh at 1 week for anti-PD-1 and healthy. Positive enrichment scores denote enrichment towards the anti-PD-1 cohort. **f**, GSEA for Hallmark gene sets for ASCs at 1 week for anti-PD-1 and healthy. Positive enrichment scores denote enrichment towards the anti-PD-1 cohort. **g**, GSEA shown for the Mitotic Spindle gene set for ICOS$^+$CD38$^+$ cTfh, ASCs and ABCs at 1 week after vaccine. Normalized enrichment score (NES) shown. **h**, GSEA for the G2M checkpoint gene set with NES is shown. **i**, GSEA plot shown for the IL-2/STAT5 pathway in the MSigDB Hallmark database for ICOS$^+$CD38$^+$ cTfh. FDR, false discovery rate.

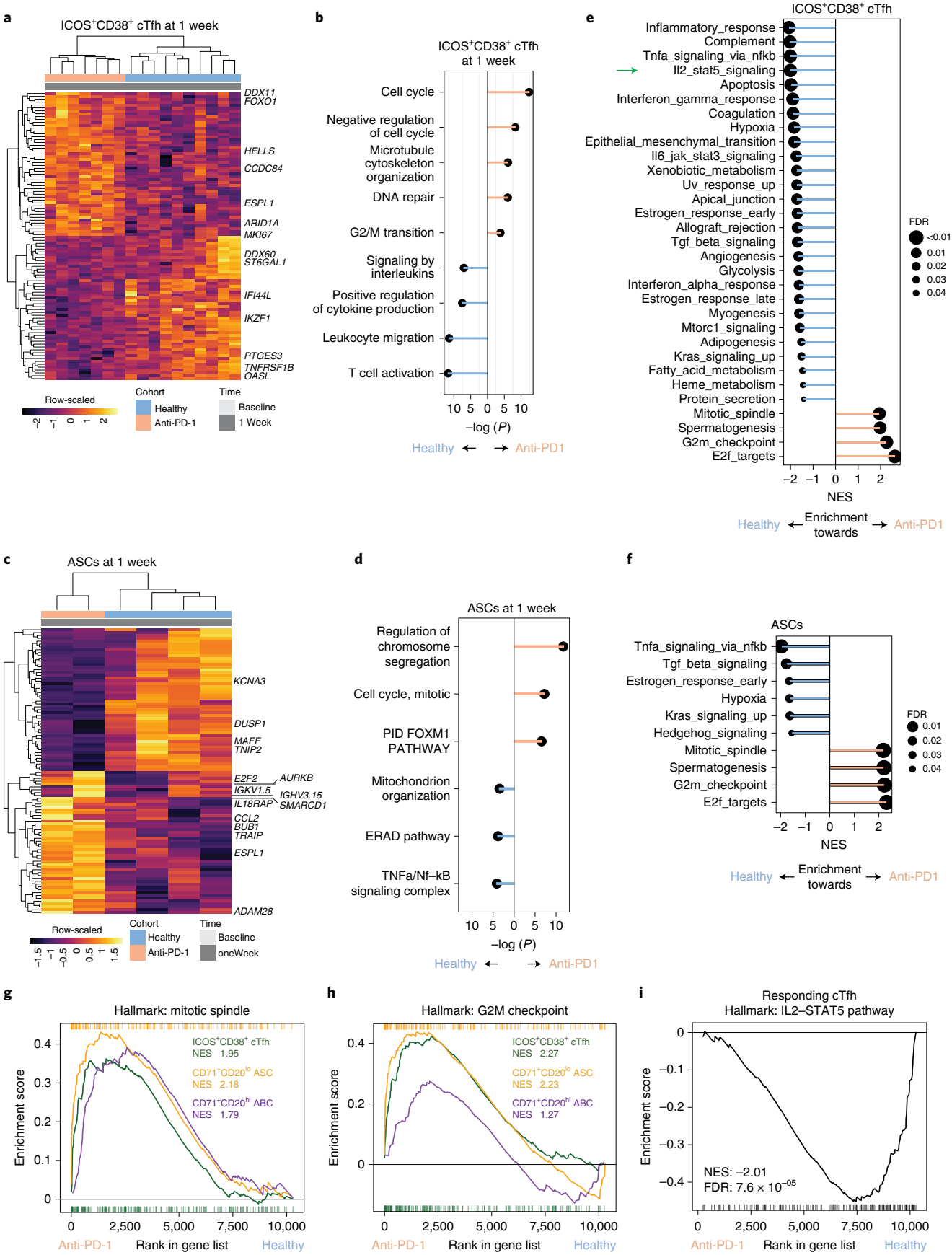
a
ICOS+CD38+ cTfh at 1 week
DDX11
FOXO1
HELLS
CCDC84
ESPL1
ARID1A
MKI67
DDX60
ST6GAL1
IFI44L
IKZF1
PTGES3
TNFRSF1B
OASL
Row-scaled
Cohort
Healthy
Anti-PD-1
Time
Baseline
1 Week
b
ICOS+CD38+ cTfh at 1 week
Cell cycle
Negative regulation of cell cycle
Microtubule cytoskeleton organization
DNA repair
G2/M transition
Signaling by interleukins
Positive regulation of cytokine production
Leukocyte migration
T cell activation
10 5 0 5 10
–log (P)
Healthy
Anti-PD1
e
ICOS+CD38+ cTfh
Inflammatory_response
Complement
Tnfa_signaling_via_nfkb
Il2_stat5_signaling
Apoptosis
Interferon_gamma_response
Coagulation
Hypoxia
Epithelial_mesenchymal_transition
Il6_jak_stat3_signaling
Xenobiotic_metabolism
Uv_response_up
Apical_junction
Estrogen_response_early
Allograft_rejection
Tgf_beta_signaling
Angiogenesis
Glycolysis
Interferon_alpha_response
Estrogen_response_late
Myogenesis
Mtorc1_signaling
Adipogenesis
Kras_signaling_up
Fatty_acid_metabolism
Heme_metabolism
Protein_secretion
Mitotic_spindle
Spermatogenesis
G2m_checkpoint
E2f_targets
FDR
<0.01
0.01
0.02
0.03
0.04
–2 –1 0 1 2
NES
Healthy
Enrichment towards
Anti-PD1
c
ASCs at 1 week
KCNA3
DUSP1
MAFF
TNIP2
E2F2
AURKB
IGKV1.5
IGHV3.15
IL18RAP
SMARCD1
CCL2
BUB1
TRAIP
ESPL1
ADAM28
Row-scaled
Cohort
Healthy
Anti-PD-1
Time
Baseline
oneWeek
d
ASCs at 1 week
Regulation of chromosome segregation
Cell cycle, mitotic
PID FOXM1 PATHWAY
Mitochondrion organization
ERAD pathway
TNFa/Nf–kB signaling complex
10 5 0 5 10
–log (P)
Healthy
Anti-PD1
f
ASCs
Tnfa_signaling_via_nfkb
Tgf_beta_signaling
Estrogen_response_early
Hypoxia
Kras_signaling_up
Hedgehog_signaling
Mitotic_spindle
Spermatogenesis
G2m_checkpoint
E2f_targets
FDR
0.01
0.02
0.03
0.04
–2 –1 0 1 2
NES
Healthy
Enrichment towards
Anti-PD1
g
Hallmark: mitotic spindle
ICOS+CD38+ cTfh
NES 1.95
CD71+CD20lo ASC
NES 2.18
CD71+CD20hi ABC
NES 1.79
Enrichment score
0.4
0.3
0.2
0.1
0
0 2,500 5,000 7,500 10,000
Anti-PD-1
Rank in gene list
Healthy
h
Hallmark: G2M checkpoint
ICOS+CD38+ cTfh
NES 2.27
CD71+CD20lo ASC
NES 2.23
CD71+CD20hi ABC
NES 1.27
Enrichment score
0.4
0.2
0
0 2,500 5,000 7,500 10,000
Anti-PD-1
Rank in gene list
Healthy
i
Responding cTfh
Hallmark: IL2–STAT5 pathway
Enrichment score
0
–0.1
–0.2
–0.3
–0.4
NES: –2.01
FDR: 7.6 × 10–05
0 2,500 5,000 7,500 10,000
Anti-PD-1
Rank in gene list
Healthy

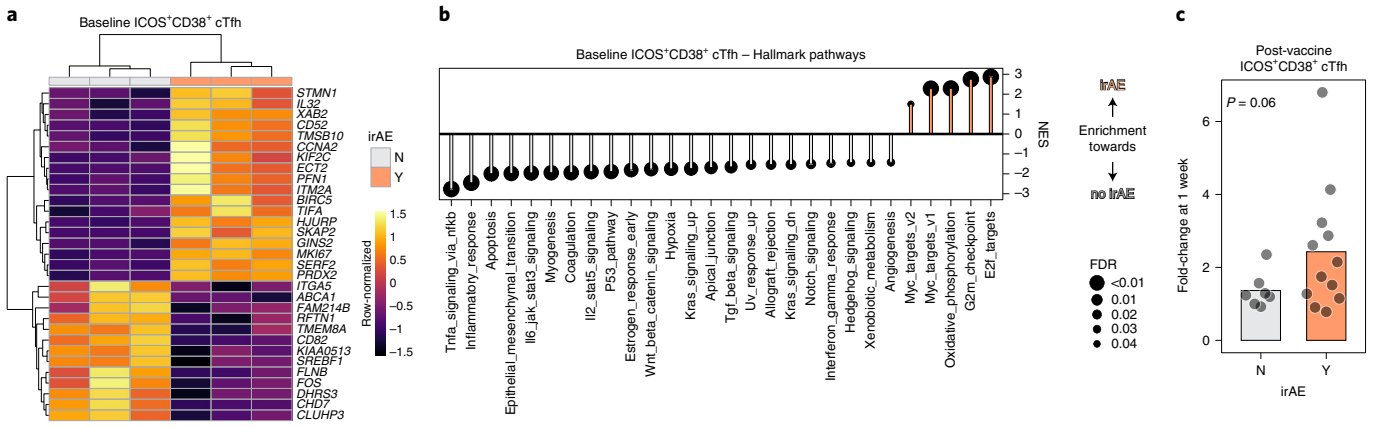

Fig. 4 | ICOS⁺CD38⁺ cTfh activation state is associated with development of irAEs. a, Anti-PD-1 participants in Cohort 2 were subgrouped based on irAEs (Y, yes; N, no). Differential expression analysis was performed on ICOS⁺CD38⁺ cTfh at baseline, and all genes with $P_{adj} < 0.05$ are shown. **b**, GSEA for Hallmark gene sets in the setting of irAE. **c**. Fold-change in cTfh responses after influenza vaccine, calculated as the frequency at 1 week relative to baseline ($P = 0.06$, two-sided *t*-test; irAE 'Yes' ($n = 12$) versus 'No' ($n = 7$)).

the global effects of PD-1 deficiency[26] and the immune-related complications of anti-PD-1 therapy, better understanding of the mechanisms of anti-PD-1 therapy on additional immune cell types is needed. Here, we exploited influenza vaccine-induced immune responses to evaluate the effects of anti-PD-1 on the Tfh–B cell axis. We identified evidence of increased early germinal centre activation which was associated with proliferation in cTfh and responding B cells. Moreover, transcriptional profiling of ICOS⁺CD38⁺ cTfh following vaccination identified key altered signaling pathways including reduced IL-2/STAT5 signaling in the setting of anti-PD-1, and these changes were associated with quantitatively robust but qualitatively impaired antibody responses to vaccination. Finally, we demonstrated that cTfh from participants with irAEs had evidence of hyper-responsiveness compared with those without irAEs.

Mechanistic studies of the in vivo effects of immunomodulators such as anti-PD-1 are challenging given limits on our ability to study immune mechanisms in humans. In previous studies, we established ICOS⁺CD38⁺ cTfh as a circulating cellular biosensor in the setting of aging[45], given that many cTfh are recent emigrants from lymphoid tissue[50,51]. Thus, platforms that employ an immunologic stimulus, particularly one widely used in routine clinical care, offer a window of opportunity to elucidate the in vivo effects of therapeutics on the Tfh–B cell axis. Indeed, little is known about the protective effects of vaccines used clinically in patients with cancer receiving immunologically relevant therapies. Moreover, influenza vaccination in the presence of anti-PD-1 augmented the induction of antibody, although antibody levels achieved by the late time point were similar to healthy adults. However, the antibodies generated in anti-PD-1-treated patients had reduced sialylation, a change that has implications for regulation of germinal centre responses and antibody affinity maturation[33]. Although it is currently assumed that influenza vaccination offers similar efficacy in patients receiving anti-PD-1 compared with patients not receiving checkpoint inhibitors, further studies will be needed to determine whether alternative vaccination strategies, such as use of adjuvants, high-dose vaccine or perhaps mRNA-based influenza vaccines, are needed to optimally protect patients.

One distinct aspect of using influenza vaccine for these studies is that the response to influenza vaccination likely mainly involves a recall response of previously primed memory CD4 T cells and B cells, with perhaps a smaller newly primed response depending on the year and strains of influenza virus in the vaccine[52]. Indeed, we previously observed recall responses in cTfh following successive annual vaccination[25]. It is worth noting that the impact of anti-PD-1 may differ for primary versus secondary responses[53] and deconvolving the primary versus recall responses in humans is complex, especially at 1 week following vaccination when both primary and recall responses would both already be clonally expanded. Thus, future studies, perhaps using antigens not previously encountered (for example, SARS-CoV-2 mRNA vaccines) and high-resolution multi-modal profiling using Cellular Indexing of Transcriptoms and Epitopes by Sequencing (CITE-seq[54]), should help further dissect the role of anti-PD-1 on pre-existing versus newly primed CD4 T cell and B cell responses.

A major gap in our knowledge is the inability to predict cancer treatment success or failure at the time of initiation of immunotherapy. Accurately predicting these responses requires better understanding of the mechanisms by which immunotherapies work. We identified increased Tfh and B cell responses to vaccination in the setting of anti-PD-1, and our findings are consistent with other reports of anti-PD-1 inducing Tfh proliferation[55]. Although evidence supports a major role for anti-PD-1 augmenting antitumour immunity via CD8 T cells[2], recent studies have also suggested a link between the Tfh–B cell axis and efficacy of immunotherapy[56–59]. Here, we enrolled participants who were receiving immunotherapy in the form of single-agent anti-PD-1 therapy (for example, pembrolizumab or nivolumab). This strategy has two implications. First, the immune response to initiation of anti-PD-1 therapy is dynamic and typically occurs within the first one to two cycles[2]. Thus, the patients studied here were biased towards those in whom loss of PD-1 signaling was more established, allowing the setting of treatment-induced steady-state PD-1 deficiency to be assessed. Second, because these patients on average had received seven or more cycles of immunotherapy, corresponding to 4–6 months since initiation, they were likely enriched for participants who were having a successful clinical response. This latter effect was advantageous in allowing us to study reasonably healthy patients, but is also worth noting since perhaps not all patients with cancer receiving anti-PD-1 therapy will respond the same way to vaccines. Whether use of such analytical vaccination as a measure of immune fitness will aid in determining outcomes of cancer therapy is unclear, but these data suggest that immuno-monitoring of the Tfh–B cell axis during cancer therapy could provide additional insights about overall immune health.

IrAEs lead to morbidity and premature discontinuation of therapy but are not well understood. Here, we found that patients with irAEs had evidence of greater sensitivity to anti-PD-1 in ICOS⁺CD38⁺ cTfh, compared with patients without irAEs, all of whom were receiving anti-PD-1. We also found that patients

with irAEs had more robust influenza vaccine-induced cTfh responses relative to patients without irAEs. Indeed, there is additional evidence from other studies for enhanced T cell activation in the setting of irAEs[49]. Patients with irAEs following immune checkpoint blockade often have better anti-cancer responses and better survival[60–62], suggesting broad rewiring of immunity by anti-PD-1 immunotherapy that impacts responses as diverse as those targeting tumour and self-antigens. Although the mechanisms for the increased sensitivity of cTfh and the germinal centre-dependent immune responses to anti-PD-1 identified here are not fully understood, these data are consistent with previous work identifying cTfh as sensitive readouts of underlying changes in overall immune system status[45]. Indeed, in the setting of immunotherapy, we hypothesize that coordination of germinal centre-dependent vaccine responses may serve as a proxy for understanding broader immune response regulation in the context of anti-PD-1 therapy. The coordinated response provoked by vaccination, however, may allow a temporally synchronized immune response and provide a high-resolution window into the anti-PD-1-dependent changes in underlying immune biology. Thus, the use of influenza vaccine as an analytical probe of broader immune function on anti-PD-1 therapy revealed insights into underlying immune set point, specifically for immune features and pathways that have a role in germinal centre-dependent immune responses which may include both responses to vaccination and autoimmunity.

In summary, these studies not only reveal a role for treatment with anti-PD-1 to reset the immune landscape beyond anti-cancer responses in some patients, but also suggest the potential of PD-1 pathway manipulation in anti-vaccine responses, and point to activated cTfh including in the context of an analytical vaccine to identify patients at risk of irAEs. The data presented here demonstrate the utility of immunoprofiling studies during a vaccine-induced perturbation as a means of uncovering mechanisms of immunomodulator therapy, which will have major implications for design and use of immunomodulator therapy.

Online content

Any methods, additional references, Nature Research reporting summaries, source data, extended data, supplementary information, acknowledgements, peer review information; details of author contributions and competing interests; and statements of data and code availability are available at https://doi.org/10.1038/s41590-022-01274-3.

Received: 23 June 2021; Accepted: 20 June 2022;
Published online: 28 July 2022

References

1. Waldman, A. D., Fritz, J. M. & Lenardo, M. J. A guide to cancer immunotherapy: from T cell basic science to clinical practice. *Nat. Rev. Immunol.* **20**, 651–668 (2020).
2. Huang, A. C. et al. T-cell invigoration to tumour burden ratio associated with anti-PD-1 response. *Nature* **545**, 60–65 (2017).
3. Crotty, S. T follicular helper cell differentiation, function, and roles in disease. *Immunity* **41**, 529–542 (2014).
4. Crotty, S. T. Follicular helper cell biology: a decade of discovery and diseases. *Immunity* **50**, 1132–1148 (2019).
5. Locci, M. et al. Tfh cells are highly functional and correlate with broadly neutralizing HIV antibody responses. *Immunity* **39**, 1–12 (2013).
6. Crotty, S. Follicular helper CD4 T cells (TFH). *Annu. Rev. Immunol.* **29**, 621–663 (2011).
7. Rasheed, A.-U., Rahn, H.-P., Sallusto, F., Lipp, M. & Müller, G. Follicular B helper T cell activity is confined to CXCR5^{hi}ICOS^{hi} CD4 T cells and is independent of CD57 expression. *Eur. J. Immunol.* **36**, 1892–1903 (2006).
8. Freeman-Keller, M. et al. Nivolumab in resected and unresectable metastatic melanoma: characteristics of immune-related adverse events and association with outcomes. *Clin. Cancer Res.* **22**, 886–894 (2016).
9. Haratani, K. et al. Association of immune-related adverse events with nivolumab efficacy in non-small-cell lung cancer. *JAMA Oncol.* **4**, 374–378 (2018).
10. Ishihara, H. et al. Association between immune-related adverse events and prognosis in patients with metastatic renal cell carcinoma treated with nivolumab. *Urol. Oncol.* **37**, 355.e21–355.e29 (2019).
11. Verzoni, E. et al. Real-world efficacy and safety of nivolumab in previously-treated metastatic renal cell carcinoma, and association between immune-related adverse events and survival: the Italian expanded access program. *J. Immunother. Cancer* **7**, 99 (2019).
12. Kennedy, L. B. & Salama, A. K. S. A review of immune-mediated adverse events in melanoma. *Oncol. Ther.* **7**, 101–120 (2019).
13. Weinmann, S. C. & Pisetsky, D. S. Mechanisms of immune-related adverse events during the treatment of cancer with immune checkpoint inhibitors. *Rheumatology* **58**, vii59–vii67 (2019).
14. Willsmore, Z. N. et al. B cells in patients with melanoma: implications for treatment with checkpoint inhibitor antibodies. *Front. Immunol.* **11**, 622442 (2020).
15. Läubli, H. et al. Influenza vaccination of cancer patients during PD-1 blockade induces serological protection but may raise the risk for immune-related adverse events. *J. Immunother. Cancer* **6**, 40 (2018).
16. Wijn, D. H. et al. Influenza vaccination in patients with lung cancer receiving anti-programmed death receptor 1 immunotherapy does not induce immune-related adverse events. *Eur. J. Cancer* **104**, 182–187 (2018).
17. Chong, C. R. et al. Safety of inactivated influenza vaccine in cancer patients receiving immune checkpoint inhibitors. *Clin. Infect. Dis.* **70**, 193–199 (2020).
18. Failing, J. J. et al. Safety of influenza vaccine in patients with cancer receiving pembrolizumab. *JCO Oncol. Pract.* **16**, e573–e580 (2020).
19. Bersanelli, M. et al. Influenza vaccine indication during therapy with immune checkpoint inhibitors: a transversal challenge. The INVIDIa study. *Immunotherapy* **10**, 1229–1239 (2018).
20. Bayle, A. et al. Immunogenicity and safety of influenza vaccination in cancer patients receiving checkpoint inhibitors targeting PD-1 or PD-L1. *Ann. Oncol.* **31**, 959–961 (2020).
21. Herati, R. S. et al. Circulating CXCR5^{+}PD-1^{+} response predicts influenza vaccine antibody responses in young adults but not elderly adults. *J. Immunol.* **193**, 3528–3537 (2014).
22. Bentebibel, S.-E. et al. Induction of ICOS^{+}CXCR3^{+}CXCR5^{+} TH cells correlates with antibody responses to influenza vaccination. *Sci. Transl. Med.* **5**, 176ra32–176ra32 (2013).
23. Morita, R. et al. Human blood CXCR5^{+}CD4^{+} T cells are counterparts of T follicular cells and contain specific subsets that differentially support antibody secretion. *Immunity* **34**, 108–121 (2011).
24. Obeng-Adjei, N. et al. Circulating Th1-cell-type Tfh cells that exhibit impaired B cell help are preferentially activated during acute malaria in children. *Cell Rep.* **13**, 425–439 (2015).
25. Herati, R. S. et al. Successive annual influenza vaccination induces a recurrent oligoclonotypic memory response in circulating T follicular helper cells. *Sci. Immunol.* **2**, eaag2152 (2017).
26. Good-Jacobson, K. L. et al. PD-1 regulates germinal center B cell survival and the formation and affinity of long-lived plasma cells. *Nat. Immunol.* **11**, 535–542 (2010).
27. Zuccarino-Catania, G. V. et al. CD80 and PD-L2 define functionally distinct memory B cell subsets that are independent of antibody isotype. *Nat. Immunol.* **15**, 631–637 (2014).
28. Wrammert, J. et al. Rapid cloning of high-affinity human monoclonal antibodies against influenza virus. *Nature* **453**, 667–671 (2008).
29. Sage, P. T. & Sharpe, A. H. T follicular regulatory cells. *Immunol. Rev.* **271**, 246–259 (2016).
30. Havenar-Daughton, C. et al. CXCL13 is a plasma biomarker of germinal center activity. *Proc. Natl Acad. Sci. USA* https://doi.org/10.1073/pnas.1520112113 (2016).
31. Cox, R. J. Correlates of protection to influenza virus, where do we go from here? *Hum. Vaccin. Immunother.* **9**, 405–408 (2013).
32. Wang, T. T. & Ravetch, J. V. Functional diversification of IgGs through Fc glycosylation. *J. Clin. Invest.* **129**, 3492–3498 (2019).
33. Wang, T. T. et al. Anti-HA glycoforms drive B cell affinity selection and determine influenza vaccine efficacy. *Cell* **162**, 160–169 (2015).
34. Krammer, F. The human antibody response to influenza A virus infection and vaccination. *Nat. Rev. Immunol.* **19**, 383–397 (2019).
35. Wang, T. T. et al. IgG antibodies to dengue enhanced for FcγRIIIA binding determine disease severity. *Science* **355**, 395–398 (2017).
36. Bournazos, S. et al. Antibody fucosylation predicts disease severity in secondary dengue infection. *Science* **372**, 1102–1105 (2021).
37. Ellebedy, A. H. et al. Defining antigen-specific plasmablast and memory B cell subsets in human blood after viral infection or vaccination. *Nat. Immunol.* **17**, 1226–1234 (2016).
38. Sun, Y. et al. Separase is recruited to mitotic chromosomes to dissolve sister chromatid cohesion in a DNA-dependent manner. *Cell* **137**, 123–132 (2009).

39. DeDiego, M. L., Martinez-Sobrido, L. & Topham, D. J. Novel functions of IFI44L as a feedback regulator of host antiviral responses. *J. Virol.* **93**, e01159–19 (2019).
40. Yang, E. & Li, M. M. H. All about the RNA: interferon-stimulated genes that interfere with viral RNA processes. *Front. Immunol.* **11**, 605024 (2020).
41. Sanmamed, M. F. et al. A burned-out $CD8^+$ T-cell subset expands in the tumor microenvironment and curbs cancer immunotherapy. *Cancer Discov.* **11**, 1700–1715 (2021).
42. Subramanian, A. et al. Gene set enrichment analysis: a knowledge-based approach for interpreting genome-wide expression profiles. *Proc. Natl Acad. Sci. USA* **102**, 15545–15550 (2005).
43. Johnston, R. J., Choi, Y. S., Diamond, J. A., Yang, J. A. & Crotty, S. STAT5 is a potent negative regulator of TFH cell differentiation. *J. Exp. Med.* **209**, 243–250 (2012).
44. Johnston, R. J. et al. Bcl6 and Blimp-1 are reciprocal and antagonistic regulators of T follicular helper cell differentiation. *Science* **325**, 1006–1010 (2009).
45. Herati, R. S. et al. Vaccine-induced $ICOS^+CD38^+$ circulating Tfh are sensitive biosensors of age-related changes in inflammatory pathways. *Cell Rep. Med.* **2**, 100262 (2021).
46. Martinov, T. et al. Programmed death-1 restrains the germinal center in type 1 diabetes. *J. Immunol.* **203**, 844–852 (2019).
47. Das, R. et al. Early B cell changes predict autoimmunity following combination immune checkpoint blockade. *J. Clin. Invest.* **128**, 715–720 (2018).
48. Gallo, P., Centonze, D. & Marrosu, M. G. Alemtuzumab for multiple sclerosis: the new concept of immunomodulation. *Mult. Scler. Demyelinating Disord.* **2**, 7 (2017).
49. Jing, Y. et al. Multi-omics prediction of immune-related adverse events during checkpoint immunotherapy. *Nat. Commun.* **11**, 4946 (2020).
50. Vella, L. A. et al. T follicular helper cells in human efferent lymph retain lymphoid characteristics. *J. Clin. Invest.* **129**, 3185–3200 (2019).
51. Sage, P. T. et al. Circulating T follicular regulatory and helper cells have memory-like properties. *J. Clin. Invest.* **124**, 5191–5204 (2014).
52. Turner, J. S. et al. Human germinal centres engage memory and naive B cells after influenza vaccination. *Nature* **586**, 127–132 (2020).
53. Shi, J. et al. PD-1 controls follicular T helper cell positioning and function. *Immunity* **49**, 264–274.e4 (2018).
54. Mimitou, E. P. et al. Multiplexed detection of proteins, transcriptomes, clonotypes and CRISPR perturbations in single cells. *Nat. Methods* **16**, 409–412 (2019).
55. Satpathy, A. T. et al. Massively parallel single-cell chromatin landscapes of human immune cell development and intratumoral T cell exhaustion. *Nat. Biotechnol.* **37**, 925–936 (2019).
56. Helmink, B. A. et al. B cells and tertiary lymphoid structures promote immunotherapy response. *Nature* **577**, 549–555 (2020).
57. Cabrita, R. et al. Tertiary lymphoid structures improve immunotherapy and survival in melanoma. *Nature* **577**, 561–565 (2020).
58. Petitprez, F. et al. B cells are associated with survival and immunotherapy response in sarcoma. *Nature* **577**, 556–560 (2020).
59. Hollern, D. P. et al. B cells and T follicular helper cells mediate response to checkpoint inhibitors in high mutation burden mouse models of breast cancer. *Cell* **179**, 1191–1206.e21 (2019).
60. Sato, K. et al. Correlation between immune-related adverse events and efficacy in non-small cell lung cancer treated with nivolumab. *Lung Cancer* **115**, 71–74 (2018).
61. Grangeon, M. et al. Association between immune-related adverse events and efficacy of immune checkpoint inhibitors in non-small-cell lung cancer. *Clin. Lung Cancer* **20**, 201–207 (2019).
62. Ricciuti, B. et al. Impact of immune-related adverse events on survival in patients with advanced non-small cell lung cancer treated with nivolumab: long-term outcomes from a multi-institutional analysis. *J. Cancer Res. Clin. Oncol.* **145**, 479–485 (2019).

Methods

Human subjects. Participants were recruited and underwent informed consent between 2015 and 2019 at the Memorial Sloan Kettering Cancer Center (Cohort 1) and at the University of Pennsylvania (Cohort 2), in accordance with the Institutional Review Boards of each institution, also described in NCT03346772 and NCT03315975. Participants were eligible if they required influenza vaccine for routine care and had not received influenza vaccine in the previous 6 months; they were excluded if they had contraindications to influenza vaccine, or needed immunosuppressive medications (that is, corticosteroids). Participants received influenza vaccine on the same day as their scheduled dose of anti-PD-1. In Cohort 1, participants under age 65 received Flulaval quadrivalent vaccine (GlaxoSmithKline), whereas participants over age 65 received Fluzone High-Dose quadrivalent vaccine (Sanofi-Pasteur). In Cohort 2, healthy adults received Fluzone quadrivalent vaccine (GlaxoSmithKline) and anti-PD-1 adults received quadrivalent vaccine (manufacturer information unavailable). Participants were compensated for their participation for visits not linked to usual care.

Peripheral venous blood was drawn at baseline (day 0), at 1 week (days 7–10) and late (21–28 d) after seasonal inactivated influenza vaccination. Blood was collected into heparinized tubes. Plasma was isolated by centrifugation, and peripheral blood mononuclear cells (PBMCs) were isolated using Ficoll-Paque PLUS (GE Healthcare) or Sepmate (Stem Cell) tubes. Participants in influenza vaccine studies in the setting of aging were described previously[21].

Flow cytometry. PBMCs were stained for surface proteins for 20 min at 25 °C. Permeabilization was performed using the Intracellular Fixation/Permeabilization Concentrate and Diluent kit (ThermoFisher) for 20 min at 25 °C. Intracellular staining was performed for 60 min at 25 °C. Antibodies and clones are described in Supplementary Table 3. Cells were resuspended in 1% para-formaldehyde until acquisition on a BD Symphony A5 cytometer. Fluorescence-minus-one controls were performed in pilot studies.

RNA-sequencing processing. PBMCs were sorted on a BD Aria II cell sorter using FACSDiva (v.8.0), followed by total RNA extraction by RNeasy Micro Plus kit (Qiagen) into DNA LoBind tubes (Eppendorf) in randomly allocated small batches. Samples were randomly distributed throughout a 96-well skirted twin.tec PCR plate (Eppendorf), followed by polyA amplification with SMART-Seq HT kit (Clontech) according to manufacturer instructions. Libraries were prepared using the Nextera XT Library Preparation kit (Illumina) using the protocol modification recommended by the Clontech kit. Libraries were indexed with a unique dual indexing strategy (IDT for Illumina Nextera DNA Set A, Illumina) to account for index hopping. Sequencing was performed on an Illumina Novaseq 6000, using 51 + 10 + 10 + 51 run geometry. FASTQ files were trimmed with Trimmomatic (v.0.32) and assessed for quality with FastQC. Libraries were aligned using STAR (v.2.5.2a) and normalized by PORT (https://github.com/itmat/Normalization/, v.0.8.5) against the GRCh38 reference assembly of the human genome. One of the 89 resultant libraries was excluded from further analysis due to poor sequencing (tenfold fewer reads than next least sample).

RNA-sequencing analysis. Variance-stabilizing transformation and differential expression were performed using *DESeq2* (v.1.28.1) based on genes with at least 20 counts in at least 25% of all libraries, using the R environment (v.4.0.2). Plots were made by *ggplot2* (v.3.3.2). Heatmap colouring was based on the 'inferno' colour-scheme from the viridis library. *t*-SNE maps were produced using *Rtsne* (v.0.15) from the variance-stabilized counts data. GO was performed using Metascape (https://metascape.com). GSEAs were performed with at least 10,000 permutations of pre-ranked GSEA (http://software.broadinstitute.org/gsea/downloads.jsp), and gene set variation analysis[63] was performed with the *GSVA* library (v.1.36.2).

Influenza-specific antibodies. The two influenza A vaccine strains of the 2014/2015 seasonal influenza vaccine, A/California/7/2009 (H1N1) pdm09-like virus and A/Victoria/361/2011 (H3N2)-like virus, were obtained from the Centers for Disease Control and Prevention (Atlanta, GA, USA). Influenza B strain B/Brisbane/33/2008 was obtained from BEI Bioresources (NR-42006). Assays to detect hemagglutinin inhibition (HAI) antibody titers were performed as previously described[33]. Infectious virus was used for neutralizing antibody assays or inactivated by β-propiolactone for H1N1/California-, H3N2/Victoria- or B/Victoria-specific binding antibody ELISA assays. Nunc MaxiSorp plates were coated with 10 mg ml^{-1} influenza A/H1N1/California, A/H3N2/Victoria or B/Brisbane/33/2008 virus along with isotype standards for IgG (Athens Research and Technology) in bicarbonate buffer overnight at 4 °C. Plates were blocked with 3% BSA in PBS and incubated with heat-inactivated sera of young and elderly adults. Antibodies were detected using alkaline phosphatase-conjugated mouse anti-human IgG (Southern Biotechnology).

ELISAs. HA ELISAs were performed as described previously[33]. Negative control sera values were subtracted from readings given by test samples. Serum antibody 50% effective concentration (EC_{50}) levels were determined by nonlinear regression analysis of the serially diluted serum optical density (OD) values as calculated by GraphPad Prism. The EC_{50} takes into account both the concentration (maximum binding) and the affinity of antibodies (for example, the slope of the binding curve) and is an accurate measure of total binding which generally correlates with the endpoint titer[64]. For hi-lo affinity ELISAs, sera diluted 1:200 were incubated on plates coated with 1 μg ml^{-1} HA protein (low density) or 6 mg ml^{-1} HA (high density). The affinity of HA-specific IgG was expressed as a ratio of binding to low-density/high-density HA-coated plates[33].

Anti-nuclear antibody and dsDNA screen. Anti-nuclear antibodies were detected by ELISA (BioVision). Here, diluted patient serum (1:21) was added to the ELISA plate coated with purified nuclear antigens. The enzyme conjugate was then added to all wells and incubated for 20 min at 25 °C. Following removal and washing three times with wash buffer, 100 μl of TMB substrate was added and allowed to incubate for 10 min before adding 100 μl of stop solution. The OD of the plates was measured at 450 nm. Antibody indices were calculated per manufacturer recommendations and values >0.9 were considered positive. Similarly, anti-dsDNA antibodies were detected by quantitative ELISA (Eagle Biosciences). Briefly, the antibodies of the calibrators and control and diluted patient samples were incubated with dsDNA immobilized on the solid phase of microtiter plates. Following an incubation period of 60 min at 25 °C, unbound sample components were removed, and plates were washed three times. The bound IgG antibody complexes were detected using anti-human-IgG conjugated to horseradish peroxidase (HRP) for 30 min at 25 °C. Then, 100 μl of TMB solution was added to each of the wells and allowed to incubate for 10 min at 25 °C before the addition of 100 μl of stop solution. The OD of the solution was measured at 450 nm. A standard curve was established by plotting the antibody concentrations of the calibrators (*x* axis) and their corresponding OD values (*y* axis) measured. The antibody concentration of each specimen was then interpolated from the standard curve.

Fc glycan analysis. IgGs were isolated from serum by protein G purification. HA-specific IgGs were isolated on agarose resin (Pierce) coupled to HA protein. Total anti-H1 HA IgGs were captured on Cal/09-coupled resin. IgG Fc-associated glycans were analysed by mass spectrometry following tryptic digestion of purified IgG or on-bead IgG.

Protein samples (10 μg) enriched by Protein G beads either in-solution or on-beads in 50 mM Tris buffer pH 8.0 were denatured with 6 M guanidine HCl, reduced with 10 mM dithiothreitol at 56 °C for 45 min and alkylated with 60 mM iodoacetamide for 1 h at 25 °C in the dark. Excess iodoacetamide was quenched with 20 mM dithiothreitol for 30 min at 25 °C. The samples were diluted to a final volume of 200 μl with 50 mM ammonium bicarbonate to reduce the guanidine HCl concentration to less than 1 M. The samples were digested by adding trypsin (0.5–1 μg, Promega) at a 1:20 ratio (w/w) and incubated at 37 °C for 16 h. All samples were desalted using solid phase extraction on Sep-Pak Cartridges (Waters) and the eluted tryptic peptides were evaporated to dryness in a Speedvac SC110 (Thermo Savant) before analysis.

Liquid chromatography–tandem mass spectrometry (MS/MS) analysis for characterization of glycosylation sites was performed on an UltiMate3000 RSLCnano (Dionex) coupled with a hybrid triple quadrupole linear ion trap mass spectrometer, the 4000 Q Trap (AB SCIEX). The digested samples were reconstituted in 50 μl of 0.2% formic acid (FA), of which 2–3 μl was injected with an autosampler onto a PepMap C18 trap column (5 μm, 300 μm × 5 mm, Dionex) with 0.1% FA at 20 ml min^{-1} for 1 min, then separated on a PepMap C18 RP nano column (3 μm, 75 μm × 15 cm, Dionex) using a 60-min gradient of 10% to 35% acetonitrile (ACN) in 0.1% FA at 300 nl min^{-1}, followed by a 3-min ramp to 95% ACN–0.1% FA and a 5-min hold at 95% ACN–0.1% FA.

Mass spectrometry data acquisition was performed using Analyst 1.4.2 software (Applied Biosystems) for precursor ion scan-triggered information-dependent acquisition (IDA) analysis and enhanced mass spectrometry-based IDA analysis[65,66]. The precursor ion scan of the oxonium ion ($HexNAc^+$ at *m*/*z* 204.08) was monitored at a step size of 0.2 Da cross a mass range of *m*/*z* 400 to 1,600 for detecting glycopeptides containing N-acetylhexosamine unit. The nanospray voltage was 1.9 kV, and was used in positive ion mode for all experiments. The declustering potential was set at 50 eV and nitrogen as collision gas. In IDA analysis, after each precursor ion scan or enhanced mass spectrometry scan, and enhanced resolution scan, the two to three highest intensity ions with multiple charge states were selected for MS/MS with rolling collision energy applied for detected ions based on different charge states and *m*/*z* values. All acquired MS/MS spectra from enhanced mass spectrometry-IDA were subjected to Mascot database search. All acquired MS/MS spectra for detected glycopeptide ions by precursor ion scanning were manually inspected and interpreted with Analyst 1.4.2 and BioAnalysis 1.4 software (Applied Biosystems). The peak areas of detected precursor ions were determined by extracted chromatogram at each specific *m*/*z* representing glycopeptide isoforms. The relative quantitations of the sugar glycan isoforms of N-linked peptide ions were carried out based on precursor ion peak areas under the assumption that all sugar glycan isoforms linked to the same core peptide have identical or similar ionization efficiency.

Statistics. No statistical methods were used to predetermine sample sizes but our sample sizes are similar to those reported in previous publications[25,45].

Randomization was not performed in these observational studies. Data collection and analysis were not performed blind to the conditions of the experiments. Statistical analyses were performed with R (v.4.0.2) using the *rstatix* library (v.0.6.0) or Prism 9 (GraphPad). Data were compared using Student's *t*-test, paired *t*-test, Wilcoxon test, one-way or two-way ANOVA with Tukey post hoc analysis, or nonparametric ANOVA with Friedman's or Sidak's post-test, as indicated. Nonparametric tests were used unless data were distributed normally based on Shapiro's test of normality. All tests throughout these studies were performed as two-tailed tests with $\alpha = 0.05$. All available data were used, and no outlier analyses were performed.

Reporting summary. Further information on research design is available in the Nature Research Reporting Summary linked to this article.

Data availability

Transcriptional profiling data reported here are available at the Gene Expression Omnibus (GEO accession GSE179487). The publicly available MSigDB Hallmark database was used for pathway analysis. Data from GSE68245 were used to validate B cell transcriptional profiles. Source data are provided with this paper.

Code availability

The minimum dataset and R scripts used in analyses and figure generation are available on Zenodo (https://doi.org/10.5281/zenodo.6665441).

References

63. Hänzelmann, S., Castelo, R. & Guinney, J. GSVA: gene set variation analysis for microarray and RNA-seq data. *BMC Bioinform.* **14**, 7 (2013).
64. Andrews, S. F. et al. High preexisting serological antibody levels correlate with diversification of the influenza vaccine response. *J. Virol.* **89**, 3308–3317 (2015).
65. Zhang, S. & Williamson, B. L. Characterization of protein glycosylation using chip-based nanoelectrospray with precursor ion scanning quadrupole linear ion trap mass spectrometry. *J. Biomol. Tech.* **16**, 209–219 (2005).
66. Zhang, S. et al. Comparative characterization of the glycosylation profiles of an influenza hemagglutinin produced in plant and insect hosts. *Proteomics* **12**, 1269–1288 (2012).

Acknowledgements

We thank the participants who volunteered for our studies, as well as members of the Wherry and Ravetch laboratories who provided critical feedback in this project. This work was supported by National Institutes of Health (NIH) grants: no. AI114852 (R.S.H.), no. AI082630 (R.S.H.), no. AI158617 (R.S.H.) and no. AG047773 (R.S.H.); the Pediatric Infectious Diseases Society Fellowship Award (L.A.V.); National Center for Advancing Translational Sciences (NCATS) award no. KL2TR001879 (L.A.V.); grant no. CA230157 (A.C.H.) and the Parker Bridge Scholar Award (A.C.H.); grant nos. AI155577 (E.J.W.), AI108545 (E.J.W.), AI112521 (E.J.W.), AI082630 (E.J.W.), AI149680 (E.J.W.) and AI117950 (E.J.W.); the US Broad Agency Announcement grant no. HHSN272201100018C (to H.C.J.E. and E.J.W.), NIH contract number 75N93021C00015 (E.J.W.) and the Allen Institute for Immunology (E.J.W.); and grant nos. U19-AI142737 (J.V.R.), R35-CA196620 (J.V.R.), K08-CA248966 (D.A.K.), R01-AI145870 (J.V.R.) and P30-CA008748. Blood collection was supported by SPORE in Skin Cancer grant nos. P50-CA174523 and P50-CA221745. We thank K. Schmader and S. Doyle for their help in influenza vaccine studies. Thanks to J. Pippin and S. Grant (Children's Hospital of Philadelphia) for assistance with sequencing. We also thank the Flow Cytometry Core and the Human Immunology Core at the University of Pennsylvania for their advice and assistance in these experiments. E.J.W. is also supported by the Parker Institute for Cancer Immunotherapy which supports the cancer immunology program at UPenn. The content is solely the responsibility of the authors and does not necessarily represent the official views of the NIH. The project described was also supported in part by grant no. UL1TR001866 from NCATS Clinical and Translational Science Award (CTSA) program. The following reagent was obtained through BEI Resources, NIAID, NIH: Influenza B Virus, B/Brisbane/33/2008 (Victoria Lineage), NR-42006.

Author contributions

R.S.H., D.A.K., L.V.S., L.A.V., A.M. and S.A. Adamski designed the study, processed samples and performed flow cytometry and sequencing experiments. R.S.H., D.A.K., S.A. Apostolidis, A.C.H., R.P.S., J.V.R. and E.J.W. interpreted the data. D.A.K., S.B. and J.V.R. performed and analysed antibody assays. S.M. processed raw RNA-sequencing data. D.F.B., S.A.F., C.-H.L., R.R.K., R.J.M., J.L.W., M.H.V., T.C.M., L.M.S., O.K., A.C.H., S.M. and L.C. assisted with clinical recruitment and oversight. S.K., R.K.K. and H.C.J.E. performed antibody assays for influenza vaccine in the setting of aging. R.S.H., D.A.K., J.V.R. and E.J.W. wrote the manuscript. All authors analysed and interpreted data, discussed the results and commented on the manuscript.

Competing interests

E.J.W. is an advisor for Merck, Marengo, Janssen, Related Sciences, Synthekine and Surface Oncology. E.J.W. is a founder of Surface Oncology, Danger Bio and Arsenal Biosciences. E.J.W. has a patent on the PD-1 pathway. R.S.H.'s spouse is an employee of Merck but was not involved in the studies. A.C.H. is a consultant for Immunai and received research funding from BMS. T.C.M. has had advisory roles with Merck, Bristol-Myers Squibb, OncoSec, GigaGen and Instil Bio. D.F.B. reports consulting fees from Bristol-Myers Squibb, Merck, Genentech-Roche, AstraZeneca and Pfizer, and institutional research support from Merck, Genentech-Roche, AstraZeneca, Novartis and Bristol-Myers Squibb. S.A.F. reports consulting fees from Merck, institutional research support from AstraZeneca and Genentech/Roche, and has stock and other ownership interest in Urogen, Allogene Therapeutics, Neogene Therapeutics, Kronos Bio, Iconovir and Vida Ventures. C.-H.L. served in a consultancy or advisory role to Amgen, Bristol-Myer Squibb, Exelixis, Merck, Pfizer, EMD Serono and Eisai, and also received research funding from Bristol-Myers Squibb, Calithera, Eisai, Exelixis, Eli Lilly, Merck and Pfizer. R.J.M. served in a consultancy or advisory role for Pfizer, Novartis, Merck, Genentech/Roche, Eisai and Exelixis, and received research funding from Bristol-Myers Squibb, Merck, Pfizer, Genentech/Roche, Eisai, Exelixis and Novartis outside of the submitted work. M.H.V. had the following consulting or advisory roles: Alexion Pharmaceuticals, Calithera Biosciences, Exelixis, GlaxoSmithKline, Natera, Novartis, Pfizer; research funding: Bristol-Myers Squibb, Genentech/Roche, Pfizer; personal fees: Novartis, Takeda; travel fees: Novartis, Takeda, Eisai, AstraZeneca; honoraria: Novartis, outside of the submitted work. The remaining authors declare no competing interests.

Additional information

Extended data is available for this paper at https://doi.org/10.1038/s41590-022-01274-3.

Supplementary information The online version contains supplementary material available at https://doi.org/10.1038/s41590-022-01274-3.

Correspondence and requests for materials should be addressed to Ramin Sedaghat Herati, Jeffrey V. Ravetch or E. John Wherry.

Peer review information *Nature Immunology* thanks Katherine Kedzierska and the other, anonymous, reviewer(s) for their contribution to the peer review of this work. Primary Handling Editor: L. A. Dempsey, in collaboration with the *Nature Immunology* team. Peer reviewer reports are available.

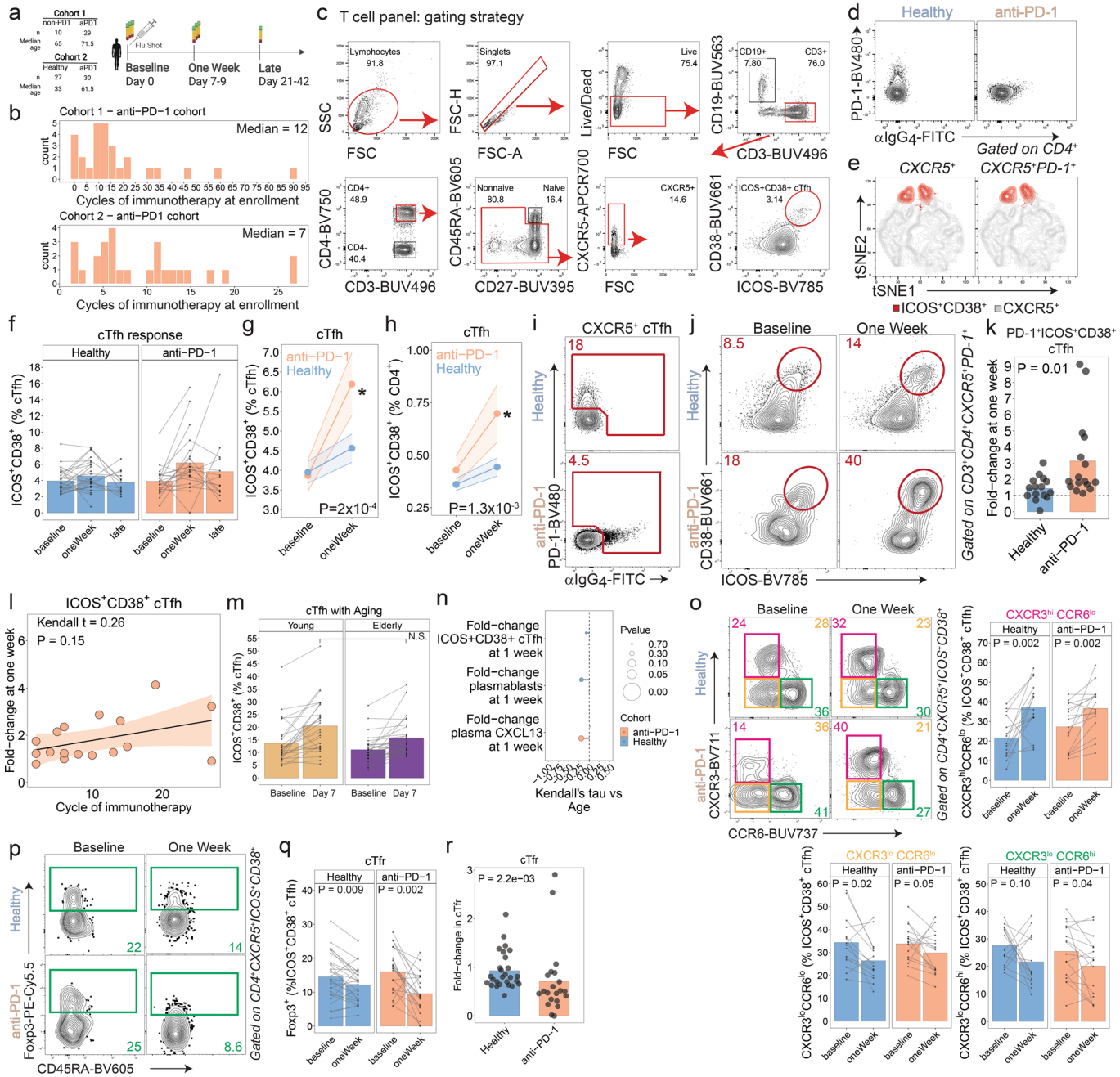

Extended Data Fig. 1 | T cell responses to vaccination. A. Study schematic. **B**. Histogram of cycle of immunotherapy shown for each cohort. **C**. Gating strategy shown for CD4 T cells. **D**. anti-PD-1 binding to cells demonstrated by absence of PD-1 staining and presence of α-human IgG4 staining. **E**. tSNE representation showing gating on ICOS$^+$CD38$^+$ either directly on CXCR5$^+$ CD4 T cells (left) or after first gating on PD-1$^+$ cells (right). **F**. ICOS$^+$CD38$^+$ cTfh responses over time. Repeat measurements from the same subjects shown as connected lines. **G**. ICOS$^+$CD38$^+$ responses shown as % cTfh ($P = 2\times10^{-4}$ for anti-PD-1 oneWeek compared to baseline; paired two-way ANOVA with Sidak's correction). Data are presented as mean values (point) ± SEM (shaded area). **H**. ICOS$^+$CD38$^+$ cTfh responses shown as % CD4 ($P = 1.3\times10^{-3}$ for anti-PD-1 at one week compared to baseline; paired two-way ANOVA with Sidak's correction). Data are presented as mean values (point) ± SEM (shaded area). **I**. PD-1 expression among CXCR5$^+$ CD4 T cells was identified by either direct staining for PD-1 or by indirect staining for α-human IgG4 staining. **J**. ICOS$^+$CD38$^+$ coexpression shown after gating on CXCR5$^+$PD-1$^+$ as identified in panel I. **K**. Fold-change in ICOS$^+$CD38$^+$ cTfh shown after gating on PD-1 as in panel J ($P = 0.01$; two-sided t-test; anti-PD-1 ($n = 16$) vs Healthy ($n = 15$)). **L**. cTfh responses vs cycle of immunotherapy for the melanoma cohort (Kendall $t = 0.26$; two-sided test; $P = 0.15$). Shaded area represents SEM by linear smoothing. **M**. An independent cohort of young and elderly adults without cancer was assessed for cTfh responses following influenza vaccination. N.S., not significant (two-way ANOVA with Tukey's post-test). **N**. Kendall correlations between the cellular responses and chronological age shown for Cohort 2. Nominal P values from two-sided test. **O**. ICOS$^+$CD38$^+$ cTfh were analysed for expression of CXCR3 and CCR6. P-values on summary plots from paired two-sided t-test comparisons. **P**. T follicular regulatory (Tfr) cells were identified among ICOS$^+$CD38$^+$ cTfh based on expression of Foxp3. **Q**. Summary plots for Tfr in Cohort 2, gated on ICOS$^+$CD38$^+$ cTfh. P values from paired two-sided Wilcoxon test without correction for multiple comparisons. **R**. Fold-change in cTfr at one week relative to baseline for Cohort 2 ($P = 2.2\times10^{-3}$; two-sided Wilcoxon test; anti-PD-1 ($n = 21$) vs Healthy ($n = 27$)).

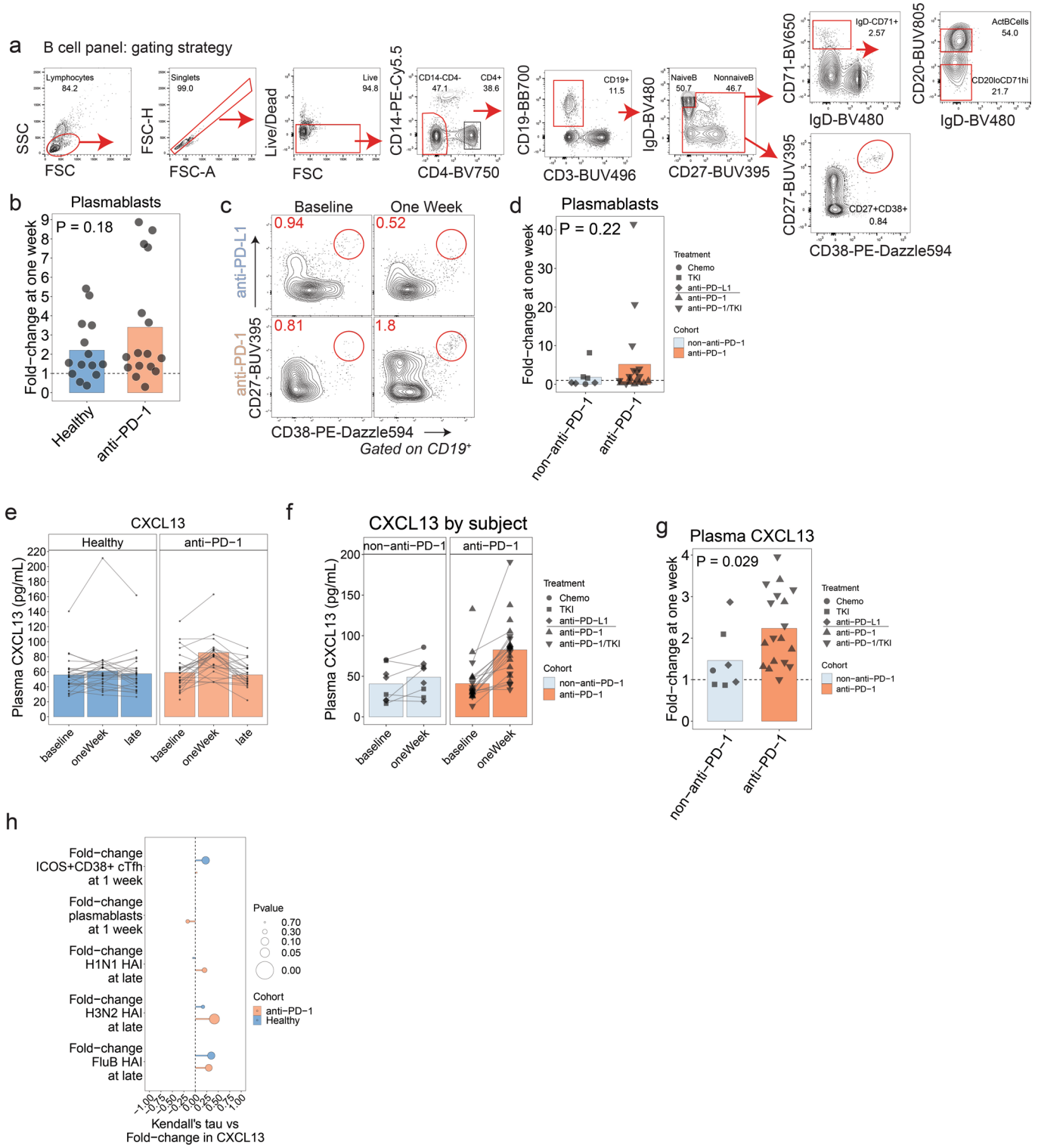

Extended Data Fig. 2 | B cell response to vaccination. A. Gating strategy for B cell analysis. **B**. Plasmablast fold-change at one week compared to baseline in Cohort 1 (P = 0.18; two-sided t-test; anti-PD-1 (n = 16) vs Healthy (n = 14)). **C**. Plasmablast responses, gated as $CD27^{++}CD38^{++}$ nonnaive $CD19^{+}$ lymphocytes in Cohort 1. **D**. Plasmablast responses shown as fold-change (P = 0.09, two-sided t-test). **E**. Plasma CXCL13 for individual subjects in Cohort 2. **F**. Plasma CXCL13 in Cohort 1. **G**. Plasma CXCL13 fold-change in Cohort 1 (P = 0.06; two-sided Wilcoxon test; anti-PD-1 (n = 18) vs non-anti-PD-1 (n = 7)). **H**. Kendall correlations between the fold-change in CXCL13 for Cohort 2 and the T, B, and humoral responses. Nominal P values from two-sided test.

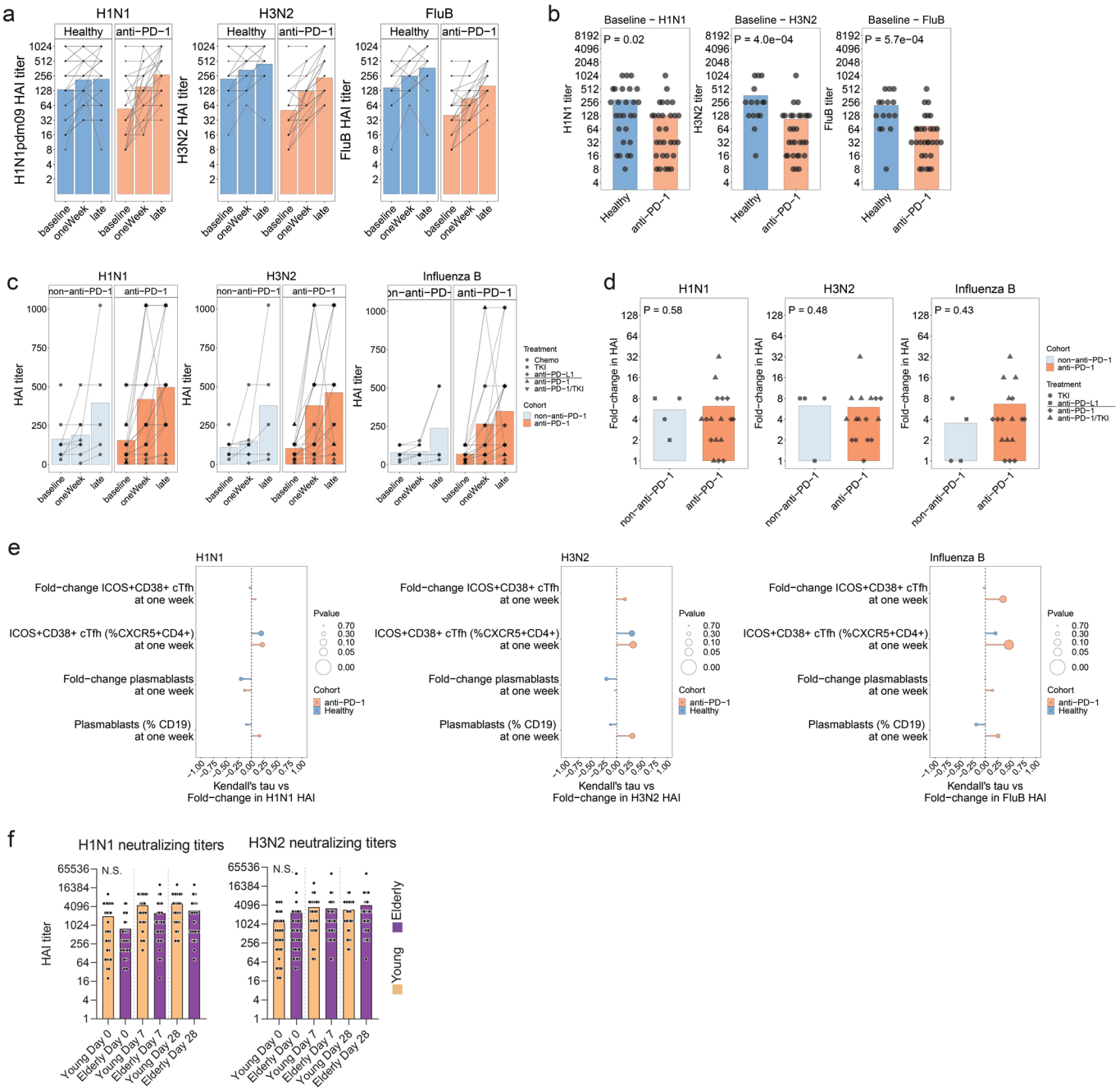

Extended Data Fig. 3 | Serological response to vaccination. A. Hemagglutinin-inhibitory titers (HAI) for three influenza virus strains for Cohort 2. Connected lines indicate repeated measurements from the same individual over time. **B**. Direct comparison of HAI titers per strain at the time of influenza vaccination for Cohort 2. P values from two-sided Wilcoxon tests. **C**. HAI titers over time for Cohort 1. Connected lines indicate repeated measurements from the same individual over time. **D**. Seroconversion as a fold-change at the late time point relative to baseline for Cohort 1. P values from two-sided Wilcoxon tests. **E**. Kendall correlations shown for the cellular responses shown versus the fold-change in HAI titer for each viral strain for Cohort 2. Nominal P values from two-sided test. **F**. HAI titers were determined in an independent cohort of young and elderly adults without cancer for H1N1 (left, Young (n = 28) vs Elderly (n = 35)) and H3N2 (right, Young (n = 28) vs Elderly (n = 35)). N.S., not significant (two-sided Mann-Whitney U-test; Young vs Elderly at day 0) for each strain.

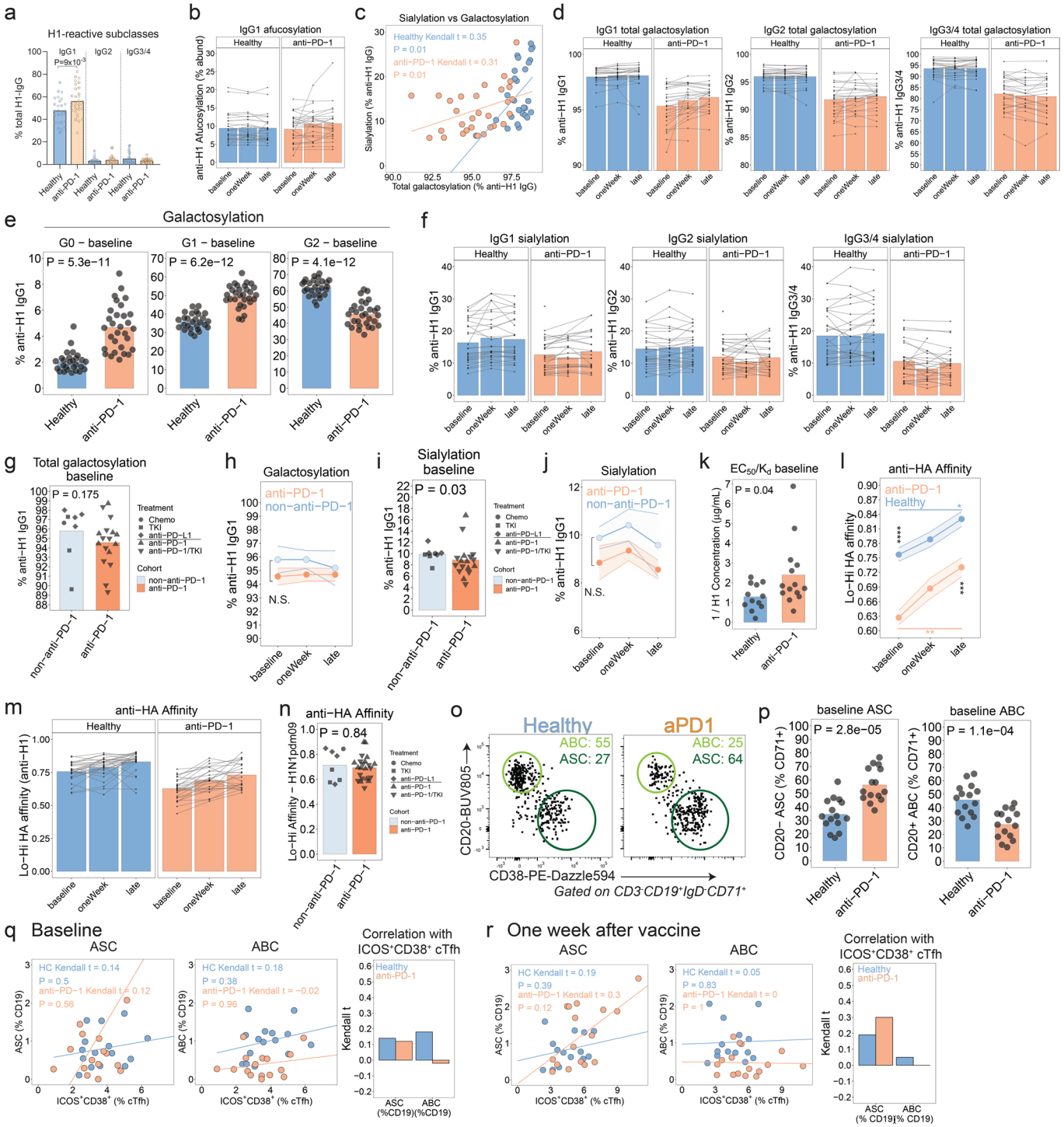

Extended Data Fig. 4 | See next page for caption.

Extended Data Fig. 4 | Antibody glycosylation and affinity studies. A. Plasma levels of IgG subclasses ($P = 9.6\times10^{-3}$ for IgG1 between Healthy and anti-PD-1; two-way ANOVA with Sidak's correction). **B**. Proportion of afucosylated anti-H1 IgG1 antibodies. **C**. Kendall correlation between sialylated anti-HA IgG1 antibodies and proportion of galactosylated anti-H1 IgG1 antibodies for Cohort 2. Nominal P values from two-sided test. **D**. Proportion of total (G1 + G2) galactosylated anti-H1 IgG1 antibodies by Ig subclass. **E**. Galactosylation shown for no galactose residues (left), one galactose residue (middle), or two galactose residues (right). P values from two-sided Wilcoxon test (anti-PD-1 (n = 30) vs Healthy (n = 27). **F**. Sialylated anti-H1 IgG1 antibodies by subclass. **G**. Total galactosylation for anti-H1 IgG1 antibodies at baseline in Cohort 1 ($P = 0.18$; two-sided Wilcoxon; anti-PD-1 (n = 17) vs non-anti-PD-1 (n = 8)). **H**. Total galactosylation for anti-H1 IgG1 antibodies over time in Cohort 1. N.S., not significant (two-way ANOVA with Tukey's). Data are presented as mean values (point) ± SEM (shaded area). **I**. Sialylation of anti-H1 IgG1 antibodies at baseline in Cohort 1 ($P = 0.03$; two-sided Wilcoxon test; anti-PD-1 (n = 17) vs non-anti-PD-1 (n = 8)). **J**. Sialylation for anti-H1 IgG1 antibodies over time in Cohort 1. Data are presented as mean values (point) ± SEM (shaded area). N.S., not significant (two-way ANOVA with Tukey's). **K**. Anti-HA affinity at baseline ($P = 0.04$; two-sided t-test; anti-PD-1 (n = 14) vs Healthy (n = 12)). **L**. Anti-HA affinity for Cohort 2, as determined by ELISA and calculated as a binding ratio of low-density to high-density of plate-bound HA protein (two-way ANOVA with Tukey's; $^{*}P = 0.02$; Healthy baseline vs late; $^{**}P = 1.7\times10^{-4}$, anti-PD-1 baseline vs late; $^{***}P = 5.0\times10^{-4}$, Healthy vs anti-PD-1 at late; $^{****}P = 4.2\times10^{-7}$, anti-PD-1 vs Healthy at baseline). Data are presented as mean values (point) ± SEM (shaded area). **M**. Anti-HA affinity over time. **N**. EC50/Kd affinity at baseline for Cohort 2 for H1N1. P value from two-sided t-test (anti-PD-1 (n = 22) vs non-anti-PD-1 (n = 8)). **O**. Examples of ASC and ABC at baseline. **P**. Baseline ASC frequencies ($P = 2.8\times10^{-5}$; t-test) and ABC frequencies by cohort ($P = 1.1\times10^{-4}$; two-sided t-test) for anti-PD-1 (n = 15) vs Healthy (n = 15). **Q**. Kendall correlations at baseline between $ICOS^{+}CD38^{+}$ cTfh for ASC (left) or ABC (middle) for Cohort 2. Nominal P values from two-sided test. Bar graph shows Kendall correlation coefficients. **R**. Kendall correlations at one week after vaccine between $ICOS^{+}CD38^{+}$ cTfh for ASC (left) or ABC (middle) for Cohort 2. Bar graph shows Kendall correlation coefficients. Nominal P values from two-sided test.

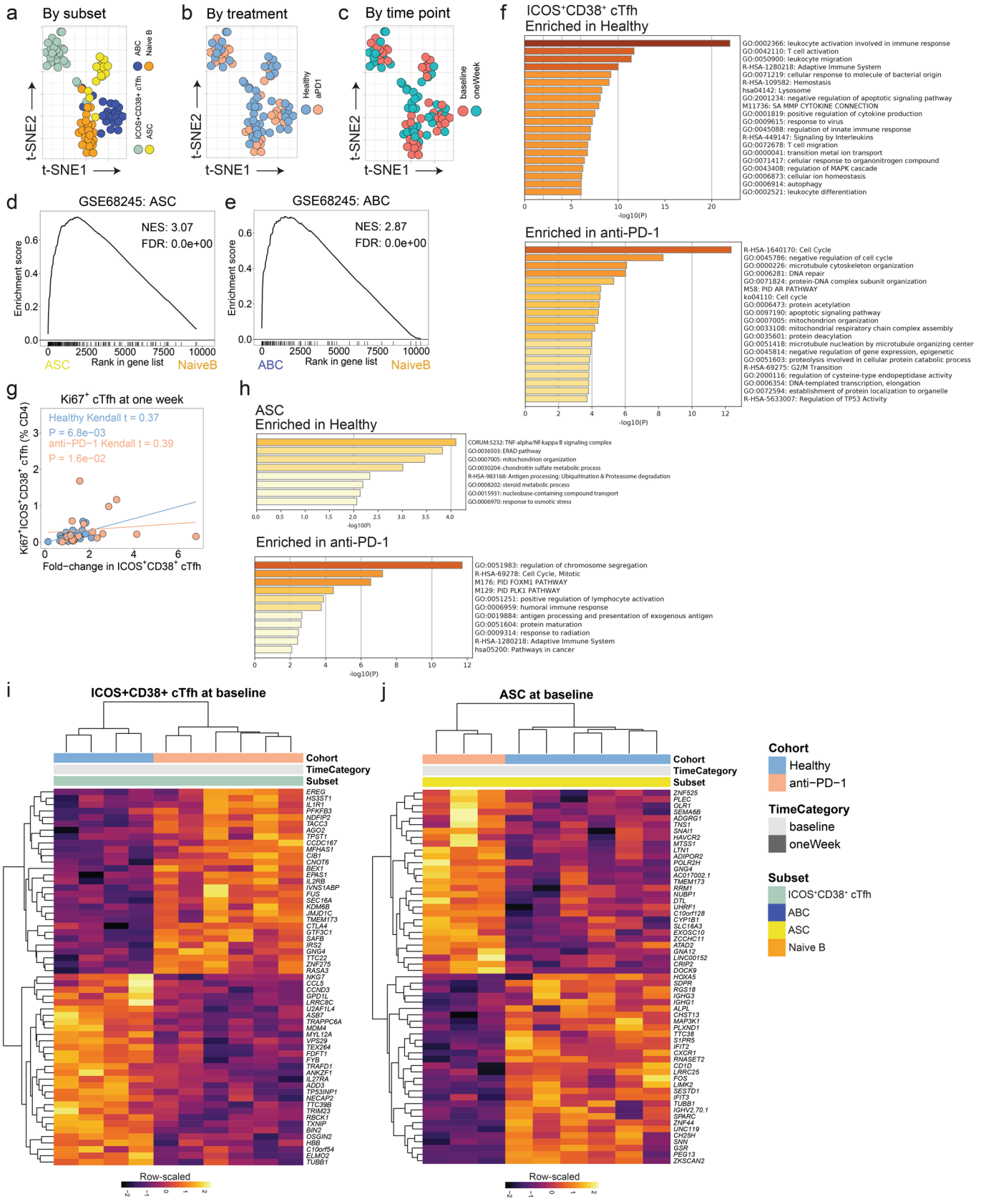

Extended Data Fig. 5 | See next page for caption.

Extended Data Fig. 5 | Differential gene expression analyses. A. tSNE for cellular subsets evaluated by bulk RNAseq. **B**. tSNE recoloured by treatment. **C**. tSNE plot recoloured by time point. **D**. ASC transcriptional profile validated against GSE68245. **E**. ABC transcriptional profile validated against GSE68245. **F**. Gene ontology for differentially expressed genes at $p < 0.01$ for $ICOS^+CD38^+$ cTfh for Healthy (top) or anti-PD-1 (bottom). P values from hypergeometric test with Benjamini-Hochberg P-value correction. **G**. Kendall correlations for the $Ki67^+ICOS^+CD38^+$ cTfh (% CD4) assessed at one week after vaccination versus the fold-change in $ICOS^+CD38^+$ cTfh at oneWeek relative to baseline. Nominal P value from two-sided test. **H**. Gene ontology for differentially expressed genes at $p < 0.01$ for ASC for Healthy (top) or anti-PD-1 (bottom). P values from hypergeometric test with Benjamini-Hochberg P-value correction. **I**. Differential expression analysis of $ICOS^+CD38^+$ cTfh at baseline. **J**. Differential expression analysis of ASC at baseline.

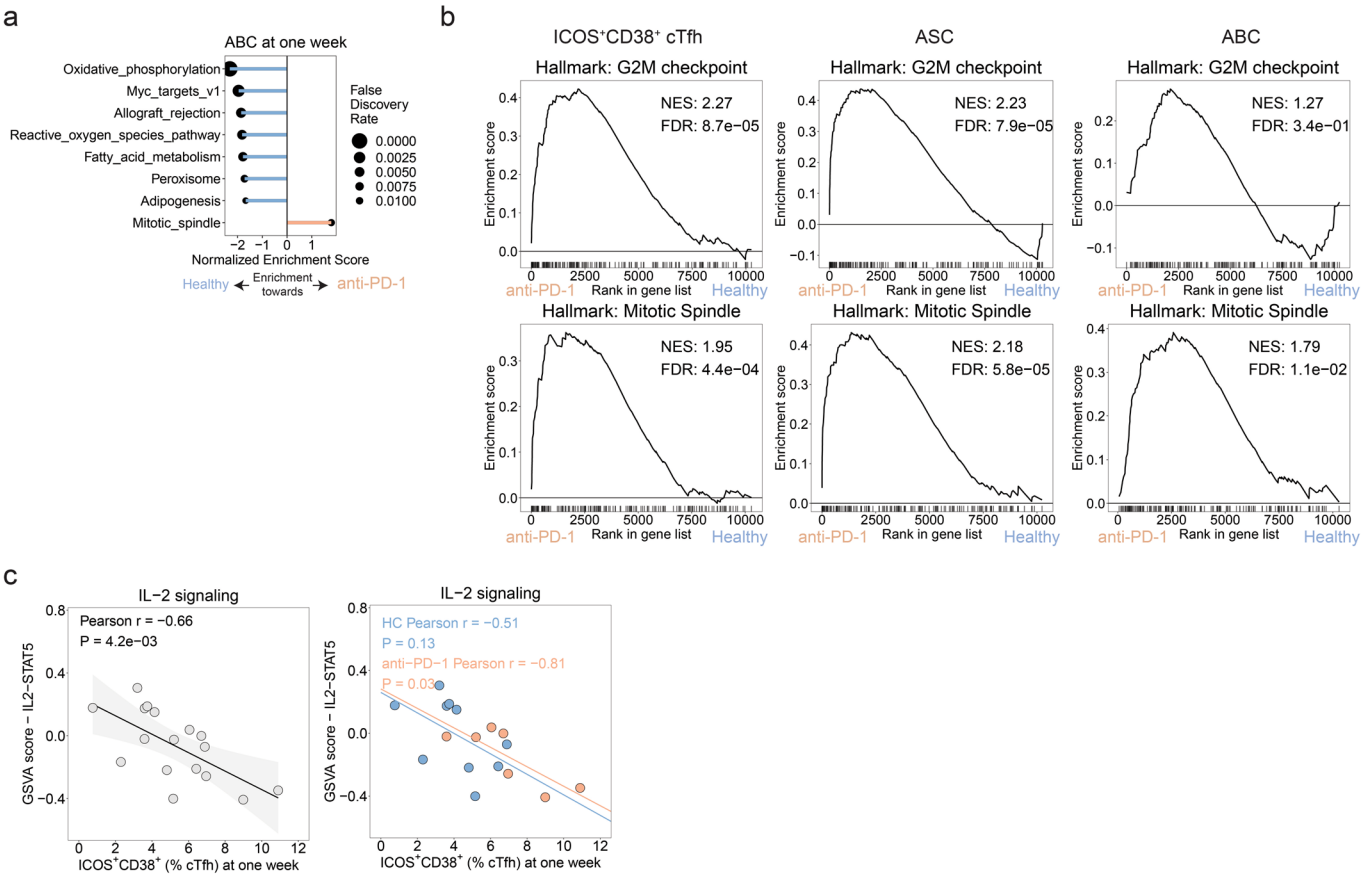

Extended Data Fig. 6 | Pathway analyses. A. GSEA for Hallmark gene sets for ABC for FDR < 0.05. **B**. GSEA plots for the G2M checkpoints and Mitotic Spindle gene sets. **C**. Pearson correlation for ICOS$^+$CD38$^+$ cTfh frequency at one week versus the GSVA score for the IL2/STAT5 gene set for ICOS$^+$CD38$^+$ cTfh at one week for the full study (left) and split by treatment group (right). P value from two-sided test.

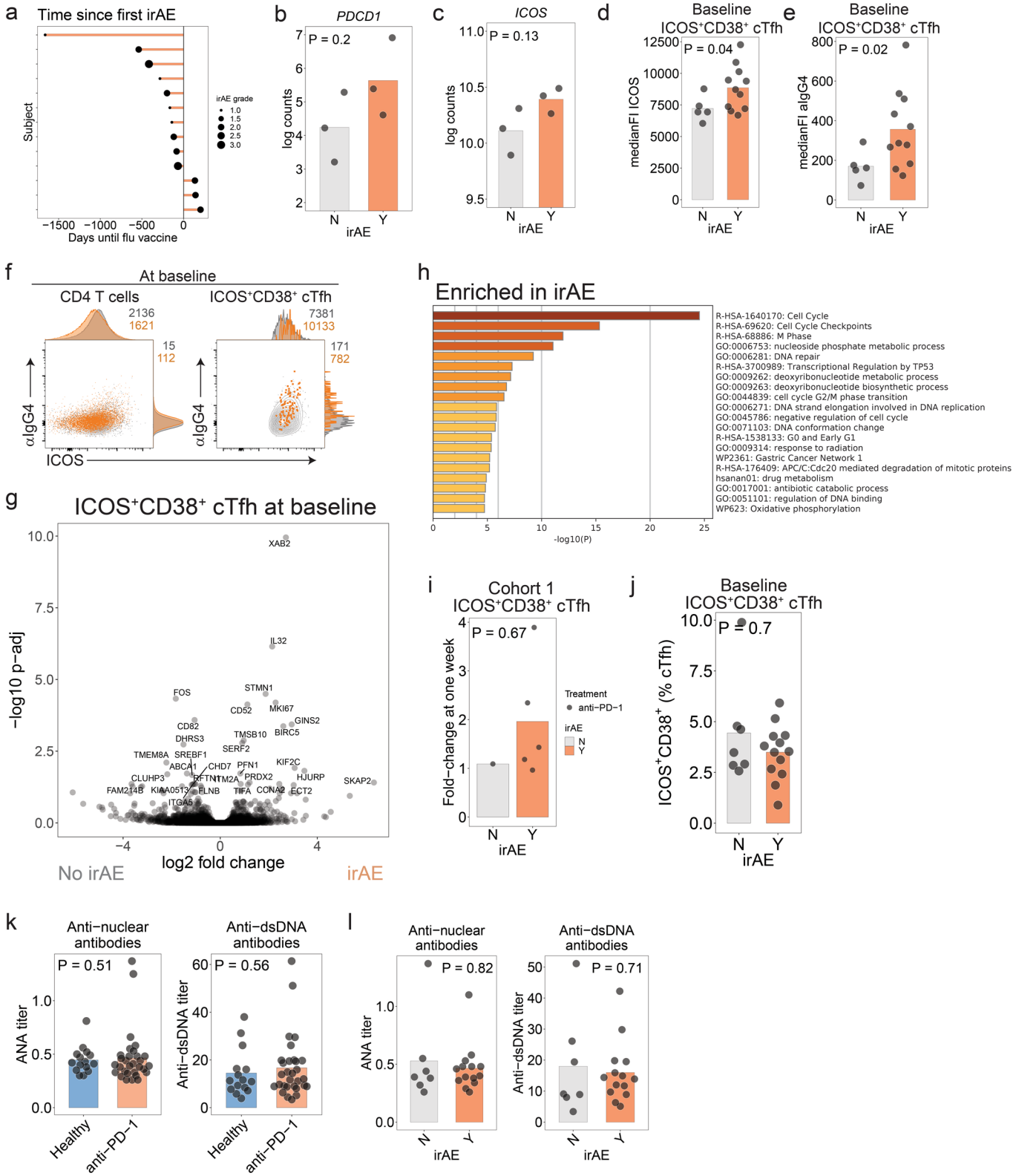

Extended Data Fig. 7 | See next page for caption.

Extended Data Fig. 7 | irAE analyses. A. Time to development of irAE in Cohort 2. **B-C**. Log-transformed counts for *PDCD1* (irAE Yes (n = 3) vs No (n = 3)) and *ICOS* (irAE Yes (n = 3) vs No (n = 3)). P values from two-sided t-test. **D**. ICOS protein in $ICOS^+CD38^+$ cTfh before influenza vaccination in Cohort 2 (P = 0.04; two-sided t-test; irAE Yes (n = 11) vs No (n = 5)). **E**. αIgG4 staining in $ICOS^+CD38^+$ cTfh before influenza vaccination in Cohort 2 (P = 0.02; two-sided t-test; irAE Yes (n = 11) vs No (n = 5)). **F**. αIgG4 and ICOS protein in total CD4 (left) or $ICOS^+CD38^+$ cTfh (right) for participants who had irAE (orange) versus those who did not have irAE (grey). **G**. Volcano plot of genes differentially expressed in anti-PD-1 cohort with respect to irAE. P values from Wald test with Benjamini-Hochberg correction. Genes labelled where Padj < 0.05. **H**. Gene ontology for genes differentially expressed at nominal P < 0.05 for $ICOS^+CD38^+$ cTfh at baseline in participants in Cohort 2 who developed irAE. P values from hypergeometric test with Benjamini-Hochberg P-value correction. **I**. Fold-change in $ICOS^+CD38^+$ cTfh at one week compared to pre-vaccination baseline in Cohort 1 (P = 0.67; two-sample t-test; irAE Yes (n = 5) vs No (n = 1)). **J**. Baseline $ICOS^+CD38^+$ cTfh frequency among those who developed irAE in Cohort 2 (irAE Yes (n = 13) vs No (n = 6)). **K**. Plasma levels of antinuclear antibodies (ANA, left, anti-PD-1 (n = 30) vs Healthy (n = 15)) and anti-dsDNA antibodies (right, anti-PD-1 (n = 30) vs Healthy (n = 15)) were assessed at baseline in Cohort 2. **L**. Plasma ANA (irAE Yes (n = 14) vs No (n = 7)) and anti-dsDNA antibodies (irAE Yes (n = 14) vs No (n = 7)).

nature portfolio

Corresponding author(s): E. John Wherry

Last updated by author(s): June 17, 2022

Reporting Summary

Nature Portfolio wishes to improve the reproducibility of the work that we publish. This form provides structure for consistency and transparency in reporting. For further information on Nature Portfolio policies, see our Editorial Policies and the Editorial Policy Checklist.

Statistics

For all statistical analyses, confirm that the following items are present in the figure legend, table legend, main text, or Methods section.

n/a	Confirmed	
☐	☒	The exact sample size (*n*) for each experimental group/condition, given as a discrete number and unit of measurement
☐	☒	A statement on whether measurements were taken from distinct samples or whether the same sample was measured repeatedly
☐	☒	The statistical test(s) used AND whether they are one- or two-sided *Only common tests should be described solely by name; describe more complex techniques in the Methods section.*
☐	☒	A description of all covariates tested
☐	☒	A description of any assumptions or corrections, such as tests of normality and adjustment for multiple comparisons
☐	☒	A full description of the statistical parameters including central tendency (e.g. means) or other basic estimates (e.g. regression coefficient) AND variation (e.g. standard deviation) or associated estimates of uncertainty (e.g. confidence intervals)
☐	☒	For null hypothesis testing, the test statistic (e.g. *F*, *t*, *r*) with confidence intervals, effect sizes, degrees of freedom and *P* value noted *Give P values as exact values whenever suitable.*
☒	☐	For Bayesian analysis, information on the choice of priors and Markov chain Monte Carlo settings
☒	☐	For hierarchical and complex designs, identification of the appropriate level for tests and full reporting of outcomes
☐	☒	Estimates of effect sizes (e.g. Cohen's *d*, Pearson's *r*), indicating how they were calculated

Our web collection on statistics for biologists contains articles on many of the points above.

Software and code

Policy information about availability of computer code

Data collection	FACSDiva (BD Biosciences, version 8.0)
Data analysis	Trimmomatic (version 0.32) STAR (version 2.5.2a) PORT (https://github.com/itmat/Normalization/, version 0.8.5) R environment (version 4.0.2) DESeq2 (version 1.28.1) ggplot2 (version 3.3.2) Rtsne (version 0.15) GSVA library (version 1.36.2) GSEA (version 4.0) rstatix (version 0.6.0) Prism 9 (Graphpad) FlowJo (BD, version 10.7.2) BioAnalysis (version 1.4) Analyst (version 1.4.2) Custom analysis scripts: doi: 10.5281/zenodo.6665441

For manuscripts utilizing custom algorithms or software that are central to the research but not yet described in published literature, software must be made available to editors and reviewers. We strongly encourage code deposition in a community repository (e.g. GitHub). See the Nature Portfolio guidelines for submitting code & software for further information.

Data

Policy information about availability of data

All manuscripts must include a data availability statement. This statement should provide the following information, where applicable:

- Accession codes, unique identifiers, or web links for publicly available datasets
- A description of any restrictions on data availability
- For clinical datasets or third party data, please ensure that the statement adheres to our policy

RNAseq data has been deposited in the NIH GEO biorepository (GSE179487). The minimum data set and custom analysis scripts are available in the Zenodo archive at 10.5281/zenodo.6665441. MSigDB Hallmark database was used for pathway analysis. Data from GSE68245 were used to validate B cell transcriptional profiles.

Field-specific reporting

Please select the one below that is the best fit for your research. If you are not sure, read the appropriate sections before making your selection.

☒ Life sciences ☐ Behavioural & social sciences ☐ Ecological, evolutionary & environmental sciences

For a reference copy of the document with all sections, see nature.com/documents/nr-reporting-summary-flat.pdf

Life sciences study design

All studies must disclose on these points even when the disclosure is negative.

Sample size	In pilot studies of cTfh responses to influenza vaccination in a small number of cancer patients compared to healthy controls, we found an effect size of f=0.397, using a one-way fixed-effects ANOVA. Because the studies were performed as observational studies (and not interventional studies), sample size targets were not established prior to the start of the study. Although sample sizes are low for the studies, we were able to replicate the central findings in two independent cohorts, totaling 96 participants overall.
Data exclusions	One RNAseq library was excluded due to poor quality. All other available data was used in the analyses.
Replication	Core findings of the study were identified in one cohort and validated using an independent, geographically-distinct cohort of patients.
Randomization	Randomization was not performed due to the observational nature of the studies. All participants received standard-of-care influenza vaccinations. Cohorts were otherwise matched for age and comorbidities. Samples were randomly allocated to small batches for RNA extraction and were randomly distributed throughout a 96-well plate for library preparation.
Blinding	All participants received influenza vaccination as per standard of care without blinding. Sample acquisition and processing was performed by technicians who were unaware of the participants' cohorts or time points. Further blinding was not possible due to the nature of the experimental set up.

Reporting for specific materials, systems and methods

We require information from authors about some types of materials, experimental systems and methods used in many studies. Here, indicate whether each material, system or method listed is relevant to your study. If you are not sure if a list item applies to your research, read the appropriate section before selecting a response.

Materials & experimental systems

n/a	Involved in the study
☐	☒ Antibodies
☒	☐ Eukaryotic cell lines
☒	☐ Palaeontology and archaeology
☒	☐ Animals and other organisms
☐	☒ Human research participants
☒	☐ Clinical data
☒	☐ Dual use research of concern

Methods

n/a	Involved in the study
☒	☐ ChIP-seq
☐	☒ Flow cytometry
☒	☐ MRI-based neuroimaging

Antibodies

Antibodies used

Antibody; Fluorochrome ; Clone; Supplier; Catalog #
CD27; BUV 395; L128; BD; 563815
CD3; BUV 496; UCHT1; BD; 564809
CD19; BUV 563; SJ25C1; BD; 565698
CD38; BUV 661; HIT2; BD; 565069

CCR6; BUV 737; 11A9; BD; 564377
CD20; BUV 805; 2H7; BD; 564917
CTLA4; BV421; BNI3; BD; 562743
PD-1; BV480; EH12.11; BD; 566112
CD16; BV510; 3G8; Biolegend; 302048
Zombie Yellow; BV570; ; Biolegend; 423103
CD45RA; BV605; HI100; Biolegend; 304133
CD25; BV650; M-A251; BD; 563719
CXCR3; BV711; G025H7; Biolegend; 353732
CD4; BV750; SK3; BD; 566355
ICOS; BV785; C398.4A; Biolegend; 313534
SLAM; A488; A12 (7D4); Biolegend; 306312
CD127; BB700; HIL-7R-M21; BD; 566398
a-mouse IgG4; PE; HP6025; Southern Biotech; 9200-09
CD28; PE-CF594; CD28.2; BD; 562296
CXCR4; PE-Cy5; 12G5; Biolegend; 306507
Foxp3; PE-Cy5.5; PCH101; Fisher; 35-4776-41
Ki67; PE-Cy7; B56; BD; 561283
Tcf1; A647; 7F11A10; Biolegend; 655204
CXCR5; APC-R700; RF8B2; BD; 565191
CD36; APC-Fire750; 5-271; Biolegend; 336220
CD25; BUV 563; 2A3; BD; 565699
CD11c; BUV 661; B-ly6; BD; 565067
CD16; BUV 737; 3G8; BD; 564433
Bcl6; BV421; K112-91; BD; 563363
IgD; BV480; IA6-2; BD; 566138
IgM; BV510; G20-127; BD; 563113
CD138; BV605; MI15; Biolegend; 356520
CD71; BV650; M-A712; BD; 743307
CD21; BV711; B-ly4; BD; 563163
CD32; FITC; FLI8.26; BD; 555448
CD19; BB700; SJ25C1; BD; 566396
CD23-biotin; BB790; M-L233; BD; 555709
CD86; PE; IT2.2; Biolegend; 305406
CD38; PE/Dazzle 594; HIT2; Biolegend; 303538
CXCR4; PE-Cy5; 12G5; Biolegend; 306507
CD14; PE-Cy5.5; TuK4; Life Technologies; MHCD1418
Tbet; PE-Cy7; 4B10; Biolegend; 644824
Blimp1; A647; 6D3; BD; 565002
CD80; APC-H7; L307.4; BD; 561134

Validation

Antibodies were validated by reviewing 1) primary data on the manufacturer's website; 2) single color titration studies using PBMC; 3) multicolor evaluation as part of the complete panel. Antibodies were verified to be reactive to human proteins and appropriate for flow cytometry applications prior to use. Further validation was performed using fluorescence minus one controls to ensure precision and accuracy of the signal.

Human research participants

Policy information about studies involving human research participants

Population characteristics	Participants with cancer were recruited from either University of Pennsylvania (n=30) or Rockefeller University (n=29) if they had a known diagnosis of either melanoma or genitourinary cancer requiring active therapy. The Rockefeller cohort participants had a median age of 65 (range 46-88) and 83% were male, whereas the University of Pennsylvania cohort participants had a median age of 61.5 (range 37 - 81) and 70% were male. Ten additional adults were recruited at Rockefeller who had genitourinary cancer but did not require checkpoint inhibitor therapy (median age 71.5, range 54-86). Healthy adults were recruited at the University of Pennsylvania with a median age of 33 (range 23-47) and 55% were male.
Recruitment	Participants for these studies were recruited by direct referral from healthcare providers and by word-of-mouth advertising. Participants were free to decline to participate in these studies, thus self-selection bias may have occurred although this would not have been expected to alter the immunological outcomes assessed here. Participants may have been enriched for those who regularly opt for annual influenza vaccination, and as a result, our results may reflect greater exposure to influenza proteins.
Ethics oversight	Approval for these studies was provided by the IRB committees of University of Pennsylvania and Rockefeller University.

Note that full information on the approval of the study protocol must also be provided in the manuscript.

Flow Cytometry

Plots

Confirm that:

☒ The axis labels state the marker and fluorochrome used (e.g. CD4-FITC).

☒ The axis scales are clearly visible. Include numbers along axes only for bottom left plot of group (a 'group' is an analysis of identical markers).

☒ All plots are contour plots with outliers or pseudocolor plots.

☒ A numerical value for number of cells or percentage (with statistics) is provided.

Methodology

Sample preparation	Peripheral blood mononuclear cells were recovered from heparinized BD vacutainers via density gradient centrifugation, followed by red blood cell lysis (ACK lysis buffer) and either immediate analysis by flow cytometery or cryopreservation in fetal bovine serum with 10% DMSO using temperature rate-controlled methods.
Instrument	Primary flow cytometry data were acquired using a BD Symphony cytometer. Cell sorting studies were conducted using a BD FACSAria II cell sorter.
Software	FACSDiva 8.0 was used to collect flow cytometry data. All subsequent analyses were performed using FlowJo version 10.7.2.
Cell population abundance	Following cell sorting, purity was checked for each sample using a small aliquot of each collected fraction. Data was acquired on the FACSAria II sorter. Samples were included in the final pooling and analysis if they demonstrated purity of at least 95%.
Gating strategy	For all samples, lymphocytes were gated based on FSC and SSC criteria, followed by identification of singlets by FSC-A vs FSC-H, followed by dead cell exclusion using Live/Dead dyes. T cells were identified by expression of CD3, whereas B cells were identified by expression of CD19. Circulating T follicular helper cells were defined as nonnaive CD3+CD4+CD8-CXCR5+PD1+.

☒ Tick this box to confirm that a figure exemplifying the gating strategy is provided in the Supplementary Information.